Aalto University
School of Chemical
Engineering

**Roshi Dahal**

# DEPENDENCE OF CARBON DIOXIDE HYDROGENATION ON THE STRUCTURE OF ZIRCONIA-BASED RHODIUM CATALYST

Master's Programme in Chemical, Biochemical and Materials Engineering
Major in Biomass Refining

Master's thesis for the degree of Master of Science in Technology
Submitted for inspection, Espoo, 22nd October, 2018

Supervisor Professor Yongdan Li

Instructor Dr. Yingnan Zhao

Aalto University
School of Chemical
Engineering

Aalto University, P.O. BOX 11000, 00076 AALTO

www.aalto.fi

**Abstract of master's thesis**

**Author** Roshi Dahal

**Title of thesis** Dependence of carbon dioxide hydrogenation on the structure of zirconia-based Rhodium catalyst

**Degree Programme** Chemical, Biochemical and Materials Engineering

**Major** Biomass Refining

**Thesis supervisor** Professor Yongdan Li

**Thesis advisor(s) / Thesis examiner(s)** Dr. Yingnan Zhao

**Date** 22.10.2018 **Number of pages** 77+3 **Language** English

## Abstract

Catalytic $CO_2$ conversion into value added products has been one of the major study due to high energy demand and increasing atmospheric $CO_2$ concentration. A catalytic reaction itself fulfills the Principles of Green Chemistry, but finding a catalyst for $CO_2$ conversion at optimal temperature and atmospheric has been a greatest challenge. Studies have shown the structure of the catalyst is vital in $CO_2$ hydrogenation for the product selectivity and reaction conditions. Support plays an important role in a reaction; where ordered structure, high surface area and active sites are of high concern for a promising catalyst. This thesis has been made to study the rely of $CO_2$ hydrogenation on the structure of the catalyst.

Support monoclinic zirconia nanorods ($ZrO_2$ NRs) were prepared via hydrothermal synthesis and Rhodium (0.5 and 2 wt%) was loaded via wet impregnation. Activity tests were conducted for carbon dioxide hydrogenation under atmospheric pressure and at 200 °C. The performance of the catalyst was compared with Rh loaded catalyst on commercial monoclinic zirconia support (com $ZrO_2$). During the experiment, the effect of parameters such as the Rhodium content and WHSV on the performance of the catalysts were compared.

200 mg of catalyst was tested in $CO_2$ hydrogenation, which was carried out for 4 h with WHSV 1500 $h^{-1}$ to 6000 $h^{-1}$. Catalyst was diluted with SiC for the higher loading of Rhodium. Catalyst prepared 0.5 wt% Rh in com $ZrO_2$ support resulted higher conversion and $CH_4$ selectivity (C = 5.23 %, $S_{CH4}$=64.9 %) than with $ZrO_2$ NRs (C = 4.7 %, $S_{CH4}$=36.9 %) . With 2 wt% Rh, $CH_4$ selectivity increased for com $ZrO_2$ supported catalyst ($S_{CH4}$=75.7 %). From the sorption experiments, the Rhodium particles were bigger in size on $ZrO_2$ NRs than on com $ZrO_2$ which could have resulted less conversion and $CH_4$ selectivity. An interesting result, with the formation of small amounts of higher alkanes (ethane, propane) during hydrogenation, was observed. The conversion and selectivity of $ZrO_2$ NRs supported catalyst could not result better than com $ZrO_2$ supported catalyst. The capping agent, NaOL, was found to be occupying the active sites on the $ZrO_2$ NRs support and thorough removal of it could result better conversion.

Nevertheless, the conversion and selectivity of zirconia-based Rhodium catalyst in $CO_2$ hydrogenation at low temperature and atmospheric pressure could open up a promising objective for the future research.

**Keywords** heterogeneous catalyst, monoclinic zirconia nanorods, hydrothermal synthesis, UV-ozone treatment, wet impregnation, Rhodium, CO2 hydrogenation, conversion, CH4 selectivity

# FOREWORD

This master's thesis has been carried out from January 2018 to October 2018 in Industrial Chemistry group at Aalto University School of Chemical Engineering. My sincere thanks for the project funding to Aalto University and The Social Insurance Institution of Finland (KELA) for providing the financial support during my Masters studies.

I would like to thank my supervisor Prof. Yongdan Li and advisor Dr. Yingnan Zhao for accepting me in this project and guidance throughout the work. My sincere thanks to Prof. Leon Lefferts for the valuable remarks and calculation corrections. Special thanks to Dr. Reeta Karinen and Dr. Tiia Viinikainen letting me over come every uncertainty and guidance throughout, thank you for being my "Guru". I would also like to thank Prof. Tapani Vuorinen for every instructions related to the teaching, and advises and directions during my masters studies.

Many thanks to Kai Cui and You Wayne Cheah for performing the sorption experiments and all the members of Industrial Catalyst group for being very helpful and friendly. I am very grateful to M.Sc. Karhan Özdenkci for reviewing my thesis for the improvement.

I am thankful to my parents and family for being my support and the driving force, words are less to express. Owing all my achievements to you!

**माता सरस्वतीकोआशिर्बाद !**

Espoo 22nd, October 2018

Roshi Dahal

# NOMENCLATURE

**Abbreviations**

| | |
|---|---|
| BET | Brunauer-Emmett-Teller |
| BJH | Barrett-Joyner-Halenda |
| DRIFTS | Diffuse reflectance infrared Fourier transform spectroscopy |
| GC-MS | Gas chromatography–mass spectrometry |
| IR | Infrared |
| m-$ZrO_2$ | Monoclinic zirconia |
| RWGS | Reverse water gas shift |
| TCD | Thermal conductivity detector |
| TEM | Transmission electron microscopy |
| TGA | Thermogravimetric analysis |
| TOF | Turn over frequency |
| UV | Ultra violet |
| WHSV | Weight hourly space velocity |
| XPS | X-ray photoelectron spectroscopy |
| XRD | X-ray diffraction |
| XRF | X-ray fluorescence |

**Symbols**

| | |
|---|---|
| $\Delta G$ | Gibbs free energy [kJ/mol] |

| | |
|---|---|
| $\Delta H$ | Enthalpy [kJ/mol] |
| nm | nanometer |
| $n_i$ | number of Carbon atoms in product *i* |
| $m_i$ | moles of product *i* |
| $m_{co2}$ | moles of $CO_2$ |
| S | Selectivity |
| wt% | Weight percentage |
| Y | Yield |

**Greek letters**

| | |
|---|---|
| $\theta$ | Diffraction angle |
| $\lambda$ | Wavelength of X-ray |

**CONTENTS**

# 1 INTRODUCTION

$CO_2$ is a sustainable source and an attractive raw material, which could be used as $C_1$ building block for organic synthesis [1]. 3 distinct major reasons (a) thermodynamics, (b) environmental demand and (c) market scope has set a high demand in $CO_2$ conversions to useful bulk products [2].

The increase in atmospheric concentration of greenhouse gases, especially carbon dioxide ($CO_2$), has been considered as one of the biggest environmental threats these days. The emissions routes of $CO_2$ mainly occurs from the combustion of carbon based fuels and chemicals processing [3]. Increased global energy demand, where the energy production relies heavily on the fossil-based fuels has been the most dominant reasons for the carbon emissions [4]. Efforts have been made to reduce carbon emissions where carbon capture approach and utilization of $CO_2$ as fuels, chemicals and reagents has rapidly increased. Such approach would benefit the planet from the environmental and economical point of view [3].

$CO_2$ conversions into fuels as methane, methanol or higher alkanes has gained major interest. $CO_2$ is highly oxidized and thermodynamically stable compound, so active metal catalyst is required to reduce it further [5]. The catalytic hydrogenation of $CO_2$ is an old process where carbon dioxide is catalytically converted into methane or even longer chains of hydrocarbons depending upon the shape and structure of the catalysts used [4]. Heterogeneous catalysts have been used to hydrogenate $CO_2$ into methane [6].

$CO_2$ hydrogenation is an exothermic reaction and methane formation is favoured at lower temperatures [1,6]. Similarly, $CO_2$ hydrogenation is sensitive to the structure of the catalyst; so a catalyst with high surface area along with nanostructured particles of metal active sites could be an optimal for this reaction [1]. Therefore, the

greatest challenge is to find a proper structured catalyst for high activity and selectivity towards methane formation at moderate temperature and pressure [7].

Support plays a vital role in a reaction because of the ability to modify the chemical behaviour of the dispersed metal and to provide thermal stability [8]. Zirconium oxide (zirconia) based catalysts has shown very interesting behaviour for $CO_2$ hydrogenation, being itself a catalyst and exhibits good features as support material [9]. Monoclinic zirconia, thermodynamically stable below at 1000 °C, is typically covered with hydroxyl groups provides versatile surface with varied surface sites [10]. Thus, the surface sites on monoclinic zirconia favours the adsorption of the reactants for the surface reaction intermediates [8,11]. Nanoparticles, in particular zirconia nanoparticles are getting more of interest due to number of key characteristics [12]. Nanoparticles have ordered pore structure, high surface area and interesting surface properties [13,14]. These chemical and physical properties of zirconia are linked with the shapes and sizes at nanometre level, and the shape/size-dependent effects of zirconia nanoparticles have been studied since decades [15].

Metal based catalysts from group VIII (Fe, Ni, Cu) and noble metal catalysts (Rh, Ru, Pt,Pd), especially Rh, have been widely studied and used for $CO_2$ hydrogenation. Rh, in particular is very active metal in the reforming of the hydrocarbon and advantageous as it favours steam reforming rather than oxidation reactions [9,16]. Nanoporous materials provides the best support for Ni, Ru, Rh, Co and Fe metal particles, preventing sintering and coking [14].

Therefore, the scope of this thesis is to study the dependence of $CO_2$ hydrogenation on the structure of the catalyst. Monoclinic zirconia nanorods will be prepared via hydrothermal synthesis, and Rh/zirconia catalyst will be prepared via wet impregnation. DRIFTS, TGA, TEM, $N_2$ physisorption, $H_2$ chemisorption, XRD, XPS and XRF will be carried out for the catalyst characterization. Finally, the catalyst will be tested in $CO_2$ hydrogenation, and the conversion and selectivity will be determined. Results will be compared with commercial monoclinic zirconia supported Rh catalyst, prepared and tested under the same conditions.

# 2 LITERATURE REVIEW

The literature part includes an overview of catalytic $CO_2$ hydrogenation, its reaction mechanism and the heterogeneous catalysts for $CO_2$ hydrogenation along with the reaction mechanism on various catalysts. The conversions and selectivity of Rhodium and zirconia based catalysts in $CO_2$ hydrogenation reviewed from different literatures and finally, monoclinic zirconia nanorods supported Rhodium catalyst as a promising one for hydrogenation along with the catalyst preparation methods is presented.

## 2.1 Catalytic $CO_2$ hydrogenation

$CO_2$ is the most oxidised state of carbon where the conversion to heavily oxygenated molecules like organic carbonates would be an easy option [2]. However, in the beginning of 20$^{th}$ century, Paul Sabatier discovered catalytic $CO_2$ hydrogenation to methane also known as Sabatier reaction which gave a new approach in $CO_2$ conversion into value added products via hydrogenation. Sabatier reaction converts carbon dioxide catalytically into methane [17,18], shown in equation 1.

$$\mathrm{CO_2} + 4\mathrm{H_2} \leftrightarrow \mathrm{CH_4} + 2\mathrm{H_2O_{(g)}} \quad \Delta H = -164 \text{ kJ/mol (at 298 K)} \qquad (1)$$

$CO_2$ hydrogenation to methane is thermodynamically favourable in producing hydrocarbons and alcohols but could be limited by the kinetics as it involves eight-electron process to convert fully oxidised $CO_2$ into methane [1, 6]. Similarly, Sabatier reaction is highly exothermic with a Gibbs free energy of $\Delta G = -130.8$ kJ/mol at 298 °C [1, 18]. In this case, a catalyst plays a very significant role in conversions and selectivity of $CH_4$. The main products from catalytic conversion of $CO_2$ are mainly fuels and chemicals, completely depends on the activity of the catalysts for the products selectivity [19], in Figure 1.

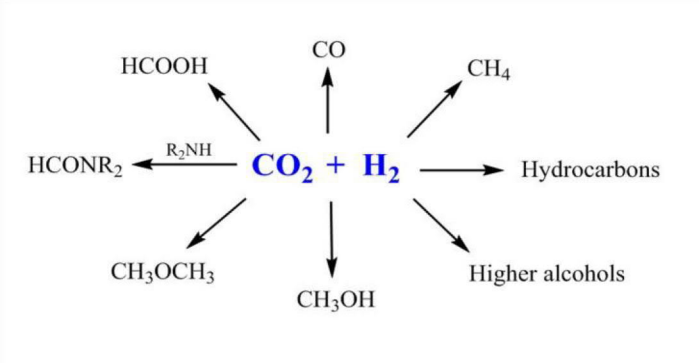


**Figure 1. Prospective products from catalytic $CO_2$ hydrogenation** [19]**.**

## 2.2 Reaction mechanism of $CO_2$ hydrogenation

Studies have been made for the reaction schemes of $CO_2$ hydrogenation, a) involving CO as an intermediate and b) direct hydrogenation of $CO_2$ [4,17–19]. Direct $CO_2$ conversion scheme suggests $CO_2$ reduction to $CH_4$ takes place via carbonate or formate intermediates without formation of any CO [4,18,20]. Involving CO as an intermediated or formate species could be another reaction route where the reaction starts with the dissociation of $CO_2$ into CO and O, also called as reverse water gas shift than follows the CO methanation [4,9,10,18,20]. It is an important reaction that occurs in the presence of $CO_2$ and $H_2$ in a reaction mixture and a key reaction occurring in catalytic conversion of carbon dioxide [19,21]. Figure 2 demonstrates both the proposed reaction mechanisms: involving and without involvement of CO as an intermediate.

Whilst, widely accepted the reaction mechanisms during $CO_2$ hydrogenation are Sabatier reaction, reverse water-gas shift reaction (RWGS) followed by further methanation of CO; presented in equations 2,3 and 4 respectively [21, 22].

$$CO_2 + 4H_2 \leftrightarrow CH_4 + 2H_2O_{(g)} \quad \Delta H = -164 \text{ kJ/mol (at 298 K)} \quad (2)$$

$$CO_2 + H_2 \leftrightarrow CO + H_2O_{(g)} \quad \Delta H = 41 \text{ kJ/mol (at 298 K)} \quad (3)$$

$$CO + 3H_2 \leftrightarrow CH_4 + H_2O_{(g)} \quad \Delta H = -206 \text{ kJ/mol (at 298 K)} \quad (4)$$

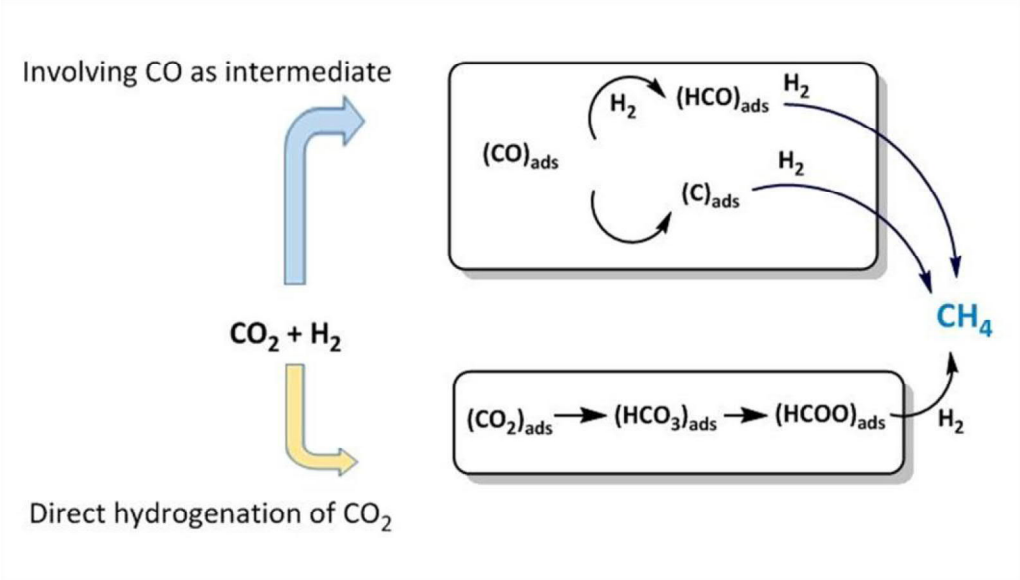


**Figure 2. Reaction mechanisms of $CO_2$ hydrogenation.**

However, the reaction steps and intermediates formation can differ depending on the active surface sites of the catalyst which will be discussed in subsection 2.3.4.

## 2.3 Heterogeneous catalysts for $CO_2$ hydrogenation

In any catalytic reaction, the high activity and selectivity of a catalyst towards reactants and products are the key concerns [17,29]. The stability of the catalysts during a reaction, performance for prolonged time and prevention of active sites poisoning are of high demand for heterogeneous catalysts [29]. The performance of the catalysts in $CO_2$ hydrogenation is dependent on various parameters, such as the effects of the support structure, metal loadings effect, catalyst preparation conditions [6].

Various oxides supports and metals have been used for $CO_2$ hydrogenation; Figure 3 presents a graphical abstract for heterogeneous catalyst. The list of heterogeneous catalysts for $CO_2$ hydrogenation with their preparation conditions is listed in Table 1.

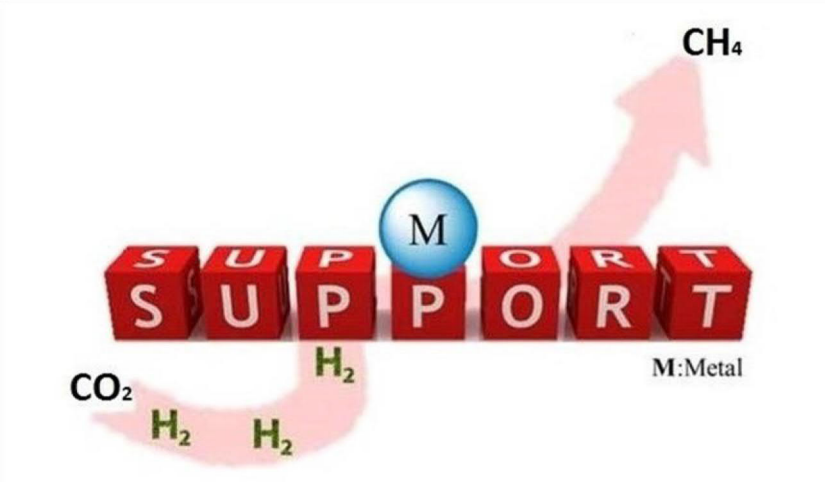


**Figure 3. A graphical abstract for $CO_2$ hydrogenation on heterogeneous catalysts** [55].

**Table 1. The list of studied $CO_2$ hydrogenation catalysts.**

| Catalyst | | Preparation methods | References | Year |
|---|---|---|---|---|
| Metal | Support | | | |
| Fe | $TiO_2$ | Impregnation | [30] | 2010 |
| Ni | $SiO_2$ | Deposition precipitation | [31] | 2018 |
| Ni | $ZrO_2$–$Al_2O_3$ | Impregnation<br>Co-precipitation<br>Impregnation-precipitation | [32] | 2011 |
| Ni | $ZrO_2$ | Impregnation | [33] | 2006 |
| Ni-Fe, Co, Cu | $ZrO_2$ | Co-impregnation | [34] | 2015 |
| Ru | $CeO_2$-$Al_2O_3$, $Al_2O_3$, $CeO_2$ | Impregnation | [35] | 2014 |
| Ni | $CeO_2$, γ–$Al_2O_3$, $TiO_2$, MgO | Impregnation | [36] | 2012 |
| Ni, Ru | $ZrO_2$ | Impregnation | [37] | 2015 |
| Cu | ZnO | Co-precipitation | [38] | 2001 |
| Pt | $Nb_2O_5$, $ZrO_2$, $TiO_2$, $SiO_2$ | Impregnation | [39] | 1986 |
| Pd | MgO, ZnO | Inverse co-precipitation | [40] | 1995 |
| Rh | $SiO_2$ | Impregnation | [41] | 1996 |
| Rh | $Al_2O_3$ | Impregnation | [23] | 2010 |
| Rh | $TiO_2$ | Impregnation | [27] | 2010 |
| Rh | $ZrO_2$ | Impregnation | [11] | 1999 |
| Rh-Fe | $Al_2O_3$ | Impregnation | [44] | 2011 |

### 2.3.1 Active component

Sabatier discovered the $CO_2$ hydrogenation where the reaction was catalyzed by Ni to convert carbon monoxide and hydrogen into methane and water [17,18]. The base metal catalysts (Fe, Co, Mo, Ni) have been studied and used for the $CO_2$ hydrogenation largely over noble metal catalysts due to cost and avaibility. Ni has been the most common active metal applied in commercial hydrogenation applications. It has high activity and is the most selective methanation catalysts [17]. The metals from the group VIII in periodic table have been used as active metals for $CO_2$ hydrogenation presented in Figure 4.

| 6 | 7 | 8 | 9 | 10 | 11 |
|---|---|---|---|---|---|
| 24 **Cr** Chromium | 25 **Mn** Manganese | 26 **Fe** Iron | 27 **Co** Cobalt | 28 **Ni** Nickel | 29 **Cu** Copper |
| 42 **Mo** Molybdenum | 43 **Tc** Technetium | 44 **Ru** Ruthenium | 45 **Rh** Rhodium | 46 **Pd** Palladium | 47 **Ag** Silver |
| 74 **W** Tungsten | 75 **Re** Rhenium | 76 **Os** Osmium | 77 **Ir** Iridium | 78 **Pt** Platinum | 79 **Au** Gold |

**Figure 4. Active metals for $CO_2$ hydrogenation marked in gray** [17]**.**

Research on Nobel metals has being in discovery of their excellent thermal stability ,lower tendency to react with support material as compared to base metals and coke resistance ability [46, 47]. The combination of Pt, Pd and Rh have been used for exhaust gas cleaning as three-way catalyst [8,48]. These catalysts are used to promote the oxidation of CO into $CO_2$, oxidation of HC into CO and water and $NO_x$ conversion into $N_2$ [8]. Rh is used for hydrogenation, selective hydrogenation, reductive amination, dry and steam reforming, carbonaylation and oxidation reactions [8,49,56]. Rh is very active in reforming hydrocarbon with the high activity than Pt

and Pd [8,16,]. At low temperatures, Ru and Rh-based catalysts have shown better activity and selectivity in $CO_2$ hydrogenation at very low temperatures, especially Rh-based catalysts at below 100 °C [23,50]. Rh is also well known metal that has catalytic activity favoring water-gas shift reaction [51,71].

### 2.3.2 Support

Support is a solid material which provides high surface area and stabilizes the dispersion of active component. Highly porous supports with high thermostability can result in high surface area and stabilize the dispersed active phase. The heterogeneous catalyst results advantageous, being a solid material and involves the active sites at the surface of solid (support) [29,49]. The better dispersion of active phase on the support material can be prepared with highly dispersed metal controlling the crystalline size.

Hydrogenation of $CO_2$ into methane can be catalyzed by noble metal catalysts Ru, Rh and Pd supported on various metal oxides [35,37,40–45]. Rh-based catalysts on various metal oxides ($Al_2O_3$, $TiO_2$, $SiO_2$, $ZrO_2$) and the activity tests in $CO_2$ hydrogenation as well as other catalytic reactions have been reported in various literature [11,23,27,41–45,52,53]. $Al_2O_3$ is very commonly used support, but rapidly suffers catalyst deactivation due to carbon deposition and cracking reactions [53]. The strong interaction of $Rh_2O_3$ and $Al_2O_3$ support in oxidizing atmosphere has been observed leading catalyst deactivation [45]. Reported in [53], the turn over frequency of $CO_2$ conversion for $TiO_2$ supported Rh catalysts increased in the following order:

Rh > Ru > Pt > Pd, where Rh was 3 times more active than Pd.

Often described as the bi-functional character of $ZrO_2$ is its capacity to adsorb $CO_2$ and $NH_3$ on its acidic and basic sites [27]. This neutralizing property leads to less carbon deposition on the support surface and zirconia is a good support for sulfur tolerance as well [8, 54]. Noble catalysts exhibit better tolerance to sulfur, especially Rh is resistance to sintering and sulfur poisoning [8,51]. $ZrO_2$ as support for noble

metals can result in better catalyst with higher stability, activity and dispersed active phase.

### 2.3.3 Principles of active sites

In the reaction mechanism of the $CO_2$ hydrogenation in the supported catalysts; support was suggested to play a role, thus determines the catalytic activity [4,6,18,19]. Mentioned earlier by Sabatier, the reaction mechanism of $CO_2$ hydrogenation could involve in formation of CO as intermediate. Involving CO as intermediate, the reaction starts from the adsorption of $CO_2$ on the catalysts surface, dissociation of $CO_2$ into CO and O and the final reaction involving $H_2$ and dissociated species and the formation of the product [23]. This leads to the principles of active sites proposed by LANGMUIR who formulated his model of chemisorption on metal surface and surface science approach to the heterogeneous catalysis [24]. Similarly, TAYLOR recognized the solid catalyst contains the edges, corners, terraces, vacancies with the sites having different coordination numbers. This difference in coordination numbers of surface atoms leads to difference in reactivity and activities of the corresponding sites [25].

This phenomenon could be studied by the catalyst characterization using in situ diffuse reflectance infrared Fourier transform spectroscopy (DRIFTS) experiments. It allows a detailed study on the surface sites on catalysts, surface species formation upon the contact to $CO_2$ on the support and the desorption behavior [19,23,26–28]. The DRIFTS spectra were compared during the adsorption of $CO_2$, CO and appearance and disappearance of different species on Rh/γ-$Al_2O_3$ catalyst at their respective wavenumbers, presented on Figure 5 [23]. From the figure, the adsorption of $CO_2$, CO and the reaction with $H_2$ as well as the formation active surface intermediates is different. DRIFTS spectra has allowed to study the reaction mechanism of the $CO_2$, CO and in the presence of H2, up on the interaction with Rh/γ-$Al_2O_3$.

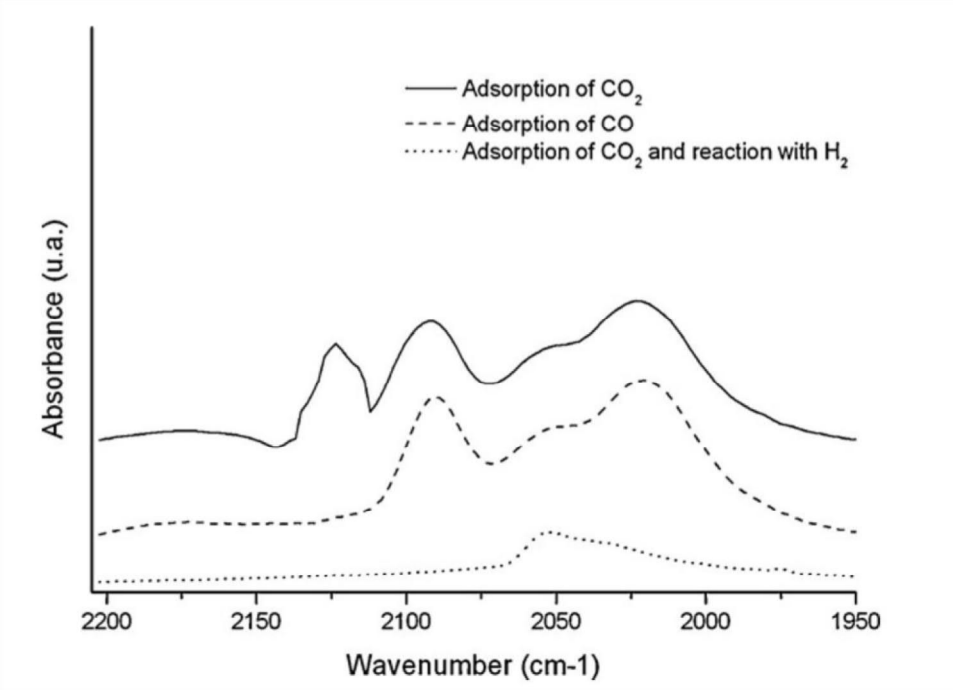


**Figure 5. DRIFTS spectra of Rh/γ-$Al_2O_3$ catalyst after adsorption of $CO_2$, CO and $CO_2$ adsorption and reaction with $H_2$** [23].

The different types of active sites on the catalyst results difference in reaction mechanism and gives rise to the formation of different intermediate species. The formation of different intermediate species can vary on the product formation as well. This phenomenon studied on the different catalysts surface will be discussed in sub-section 2.5.

### 2.3.4 Hydrogenation reaction schemes on various catalysts

Schild et al. [82], studied about the reaction mechanism of methane formation in $CO_2$ hydrogenation over $Ni/ZrO_2$ catalyst using in-situ diffuse reflectance spectroscopy. They suggested the mechanism of CO and $CO_2$ hydrogenation together along with the RWGS they observed during the reaction in Figure 6. $CO_2$ hydrogenation was proposed to form with the non-dissociative path via formate hydrogenation, whereas CO hydrogenation with dissociation rather than desorption. Further, the dissociated CO into adsorbed C species hydrogenated to methane or higher alkanes.

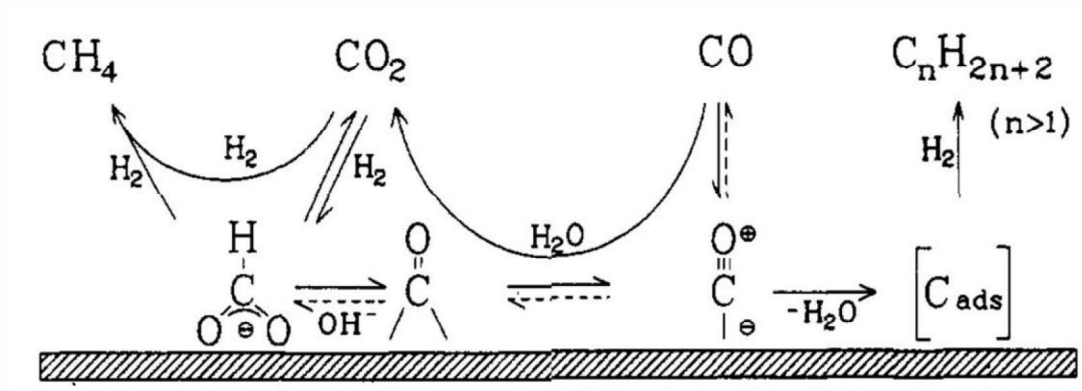


**Figure 6. Proposed reaction mechanism for CO and $CO_2$ hydrogenation over $Ni/ZrO_2$** [82]**.**

Pan et al. [83], studied the reaction mechanism of $CO_2$ hydrogenation where they proposed a mechanism where CO is not formed as an active intermediate. Using in-situ FTIR spectroscopy they found carbonates and formats as an active intermediates in $CO_2$ hydrogenation over $Ni/\gamma\text{-}Al_2O_3$, in Figure 7. Reviewed in the ref., $CO_2$ hydrogenation of $CO_2$ in $Ni/\gamma\text{-}Al_2O_3$ catalyst was followed through the formation of bidentate formate whereas, $Ni/Ce_{0.5}Zr_{0.5}O_2$ proceeded with bidentate and monodentate formate formation in Figure 8. These active intermediate species are formed depending on the reactions of $CO_2$ on different active sites.

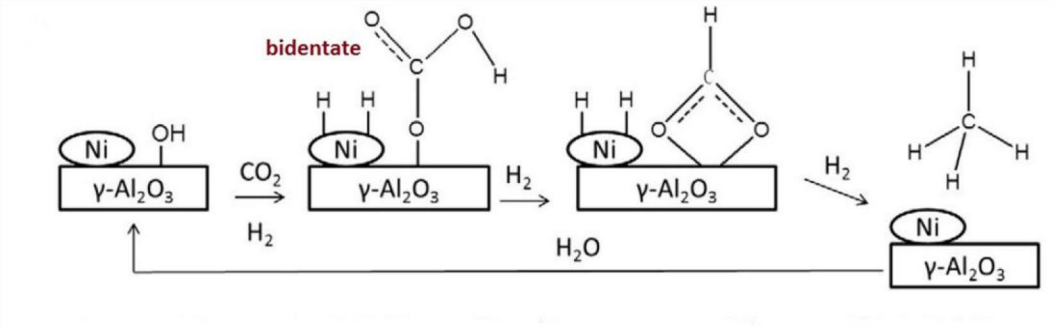


**Figure 7. Reaction mechanism with bidentate formate as intermediate for $CO_2$ hydrogenation and methane formation over Ni/γ-$Al_2O_3$** [83].

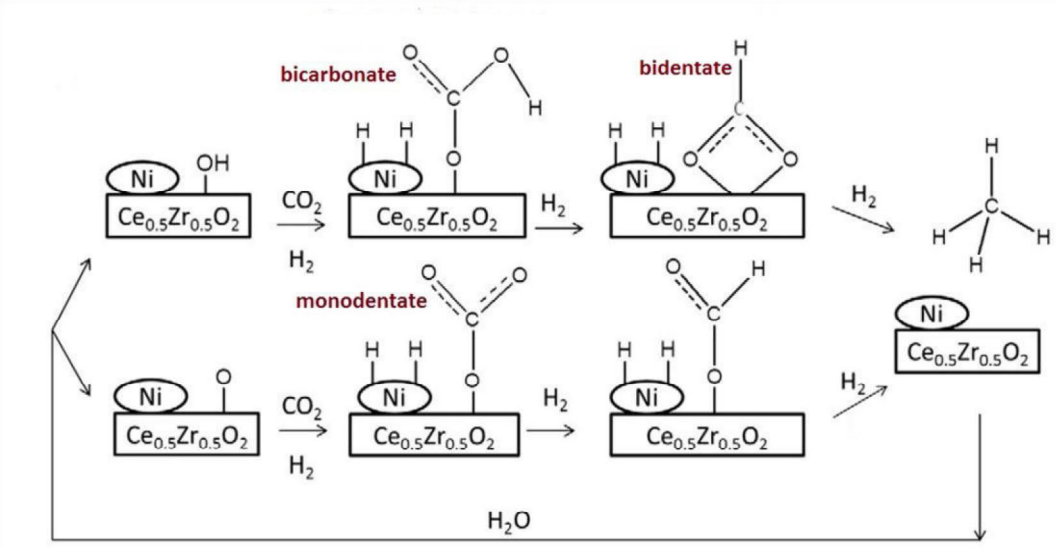


**Figure 8. Reaction mechanism with mono and bidentate formate as intermediate for $CO_2$ hydrogenation and methane formation over Ni/$Ce_{0.5}Zr_{0.5}O_2$** [83].

## 2.4 Conversions and selectivity of catalysts in $CO_2$ hydrogenation

Metal oxides especially $ZrO_2$, has been used as a catalyst and catalyst support for $CO_2$ hydrogenation. The base and noble metals in monometallic and bimetallic forms have been used for the catalyst preparation with zirconia support. The conversion and selectivity of zirconia-supported catalysts, Rh-based catalyst and Rh/zirconia catalyst in $CO_2$ hydrogenation will be reviewed in this section. The products selectivity, effects of WHSV and reaction conditions will be discussed as well.

### 2.4.1 Metal/zirconia

Ni is widely used base metal for $CO_2$ hydrogenation due to its high selectivity and low cost in comparison to noble metals. Ni catalyst with different loadings on nano $ZrO_2$ was prepared with wet impregnation, where the support nano $ZrO_2$ was prepared with self-assemble formation of sol-gel [79]. The effect of different loadings of Ni and reaction temperatures in CO and $CO_2$ methanation was studied.

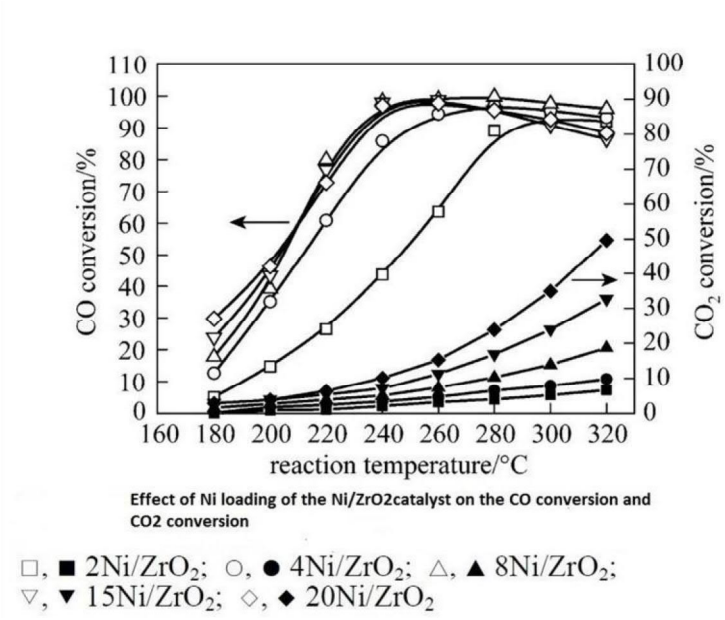


**Figure 9. CO and $CO_2$ conversion over $Ni/ZrO_2$** [79].

From Figure 9, higher conversion was achieved with lower loadings of Ni for $CO_2$ conversions. Similarly, increasing reaction temperature resulted better $CO_2$ conversions whereas all Ni loadings in the catalyst gave similar CO conversion after 300 °C. Mentioned in the article, it was a selective methanation so no other products formation was discussed.

Studies made by Lange, F. et al [37] on hydrogenation of $CO_2$ into methane, Ru and Ni catalysts on $ZrO_2$ support with different loadings were evaluated in CO2 hydrogenation at 300 °C and 10 bars with different feed compositions.

Catalytic test results at varying feed gas composition.[a]

| Catalyst | Feed gas[b] | $X(CO_2)$ [%] | $S(CH_4)$ [%] | $S(C_2H_6)$ [%] |
|---|---|---|---|---|
| 5 Ni | 1:4:5 | 96.9 | 99.8 | 0.2 |
| | 1.2:5:3.8 | 97.3 | 99.8 | 0.2 |
| | 1.5:5.8:2.7 | 97.6 | 99.8 | 0.2 |
| | 1.7:6.7:1.6 | 97.8 | 99.7 | 0.3 |
| | 1.8:7.2:1 | 97.9 | 99.7 | 0.3 |
| 3 Ru | 1:4:5 | 97.2 | 100.0 | 0 |
| | 1.2:5:3.8 | 97.6 | 100.0 | 0 |
| | 1.5:5.8:2.7 | 98.0 | 100.0 | 0 |
| | 1.7:6.7:1.6 | 98.3 | 100.0 | 0 |
| | 1.8:7.2:1 | 98.5 | 100.0 | 0 |

[a] $T = 300\,^{\circ}C$, $p = 10$ bar, GHSV $= 6000\ h^{-1}$; [b] Molar ratio of $CO_2/H_2/N_2$.

**Figure 10. $CO_2$ hydrogenation over $Ni/ZrO_2$ and $Ru/ZrO_2$** [37].

From Figure 10, the formation of the products in $CO_2$ conversion, over zirconia supported Ni and Ru catalysts, remained same even with the changing feed gas composition. Small traces of ethane was observed with $Ni/ZrO_2$ catalyst whereas, $Ru/ZrO_2$ catalyst was 100 % selective to methane. Mentioned in the article, particle size of Ni was in the range of 20-30 nm and Ru with particle size of 4 nm. Ni loading was higher than Ru on the support which could be the reason for bigger particle size. Yet, the particle size of the metal and the product formation relation cannot be predict-

ed from this result, but the change in feed gas composition did not result any impact in the product formation.

### 2.4.2 Rhodium/metal oxides

CO and $CO_2$ hydrogenation were studied over $Rh/TiO_2$ catalyst prepared by wetness impregnation with 2 % Rh [30]. 0.15 g of catalyst was tested in a fixed-bed microreactor with the total gas flow of 20 $cm^3$/min ($H_2$:$CO_2$ 1:1) at 543 K and 20 atm. The influence of temperature and WHSV on $CO_2$ conversions and product selectivity was studied. In Figure 11, $CO_2$ conversion and methane selectivity increased with increasing temperature whereas methane selectivity decreased with increasing WHSV. The $CO_2$ conversion with $Rh/TiO_2$ catalyst resulted in the formation of products such as methane, higher alkanes as ethane, propane, butane, alcohols as ethanol and methanol and small traces of acetaldehyde, in Table 2.

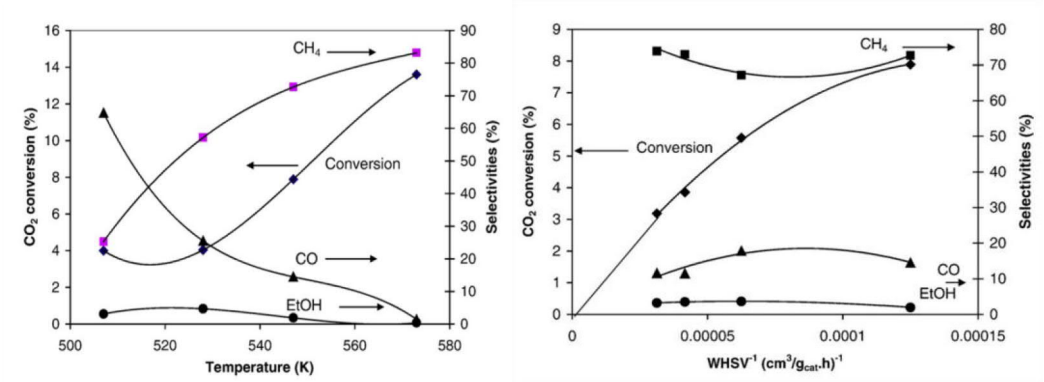


**Figure 11. Influence of temperature and WHSV on $CO_2$ conversion over $Rh/TiO_2$** [30].

**Table2 .$CO_2$ hydrogenation into methane over $Rh/TiO_2$** [30].

| | | Selctivity (%) | | | | | | | |
|---|---|---|---|---|---|---|---|---|---|
| Catalyst | Conv. (%) | $CH_4$ | $C_2H_6$ | $C_3H_8$ | $C_4H_{10}$ | $CH_3CHO$ | $CH_3OH$ | EtOH | CO |
| 2% $Rh/TiO_2$ | 7.89 | 72.7 | 4.30 | 4.10 | 0.98 | 0.67 | 0.80 | 1.93 | 14.5 |

Jacquemin et al. [23] made study on catalytic methane production from $CO_2$ and $H_2$ over $Rh/Al_2O_3$ catalyst at low temperatures. $CH_4$ was the only product formed with 100 % selectivity as reported. Fischer et al. [41] studied $CO_2$ and CO hydrogenation over $Rh/SiO_2$ where the rate of methane formation was compared with changing temperature and pressure. Methane was only the product formed as mentioned.

### 2.4.3 Rhodium/zirconia

$Rh/ZrO_2$ catalyst have been researched and used for different kinds of catalytic reactions as methane combustion and reduction of NO with propene [45], oxidation and reduction reactions [42], CO oxidation [43], steam reforming [80], biofuels production [8], including $CO_2$ hydrogenation [11]. Reported by Wambach et al.[11], originally cited in Inoue et al. [81] $Rh/ZrO_2$ catalyst used in $CO_2$ hydrogenation resulted methane as the main product.

$Rh/ZrO_2$ have been used for various reactions but very limited amount of studies investigating for $CO_2$ hydrogenation. The interesting properties of both the components could result a good catalyst for $CO_2$ hydrogenation.

## 2.5 Zirconia based catalysts

In this thesis, Rh and $ZrO_2$ will be used as catalyst for $CO_2$ hydrogenation therefore, further sections and sub-sections will discuss about the phases of $ZrO_2$, its nanostructures, active sites on monoclinic $ZrO_2$ and catalyst preparation methods.

### 2.5.1 Zirconium oxide (zirconia)

Discovered by German chemist Martin Heinrich Klaporth in 1789, Zirconium (zirconia) is a chemical element with symbol Zr and atomic number 40. It belongs to the group IV in periodic table and is very strong with the melting point 2983 K [57]. Research and development on zirconia as ceramic biomaterial had been started since 60s and being a good chemical with high thermal stability and toughness, it has still been a topic of continuous research [58]. Zirconia is ranked as the 18$^{th}$ most abundant element found on the earth's crust, yet it does not occur in pure state [59]. As reported by US Geological survey (USGS) 2017, zirconia reserves totalled 75 thousand metric tons presented in Figure 12 along with the uses of zirconia.

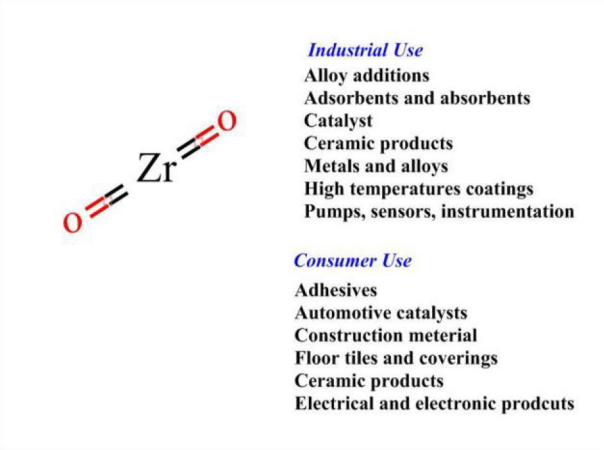


**World zirconium reserves**

(Data in thousand metric tons, $ZrO_2$)

| Country | Reserves |
|---|---|
| Australia | 48,000 |
| South Africa | 14,000 |
| India | 3,400 |
| Mozambique | 920 |
| United States | 500 |
| China | 500 |
| Other countries | 7200 |
| World total | **75,000** |

*Source: USGS, 2017*

**Figure 12. Uses of $ZrO_2$ adapted from ref [60] and World zirconium reserves** [61]**.**

The temperature dependent phase transition of pure zirconia occurs in three different crystal structures as monoclinic, tetragonal and cubic in Figure 13 [62,63]. Dopants are used for stabilizing the structures of $ZrO_2$ as the structure transformation occurs on heating [62]. The monoclinic phase is stable at lower temperatures below 1000 °C as tetragonal phase is favoured at higher temperatures above 2300 °C [63].

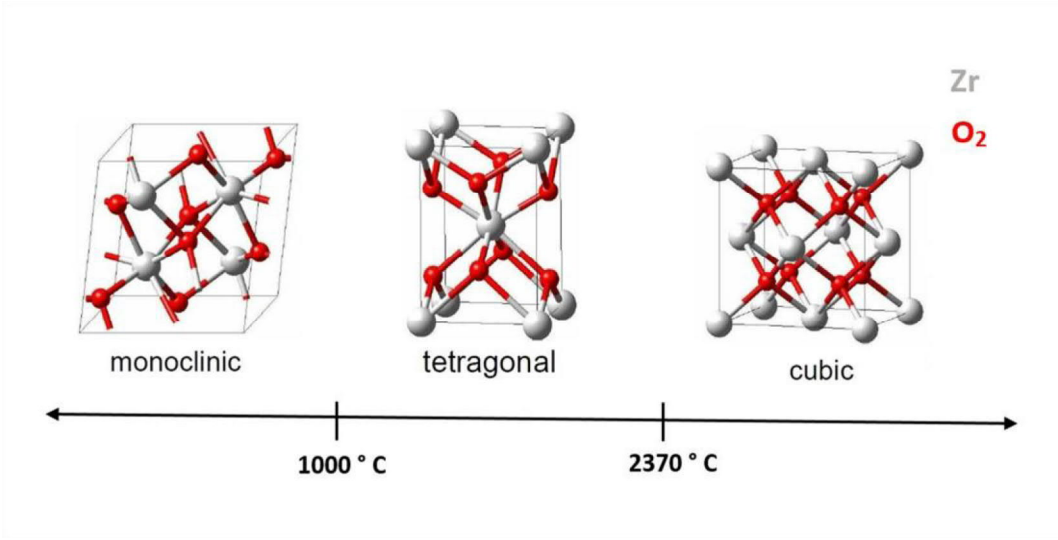


**Figure 13. Phases of $ZrO_2$ at different temperatures** [63]**.**

### 2.5.2 Monoclinic zirconia

Monoclinic zirconia ($ZrO_2$) also known as baddeleyite occurs as natural mineral and is the most stable phase below 1000 ° C. Typically covered with hydroxyl groups in this phase, the surface sites of monoclinic zirconia are hydroxyl groups, oxygen vacancies, unsaturated Zr-O pairs and Lewis acid centres ($Zr^{3+}$, $Zr^{4+}$). In crystal form, monoclinic zirconia has nine crystalline directions as [001], [010], [100], [101], [011], [101], [111] and [111]. The most stable surface is [111] surface of monoclinic zirconia. [10]

The surface hydroxyl groups play a very important role in the interaction with CO and $CO_2$ with zirconia as active sites, for the formation of formates and bicarbonates respectively. The crystal structure of zirconia is one of the significant factors in determining the nature and amount of surface sites that is suitable for $CO_2$ adsorption [64]. The monoclinic phase being more symmetrical than amorphous and tetragonal possess varied surface surfaces and surface sites. Thus, leading to the greater $CO_2$ surface adsorption [10,64].

In Figure 14 [25], monoclinic and tetragonal zirconia samples have been used to study the adsorption of $CO_2$ using DRIFTS at increasing temperatures (373–573 K). A clear effect of support surface structure is observed on the adsorbed species of $CO_2$ at respective wavenumbers and their intensities. Hereby, it can be concluded the polymorphs of zirconia exhibit difference in surface sites and structures [9,10]; versatility in monoclinic phase. During this thesis, monoclinic zirconia supports were used for the catalyst preparation.

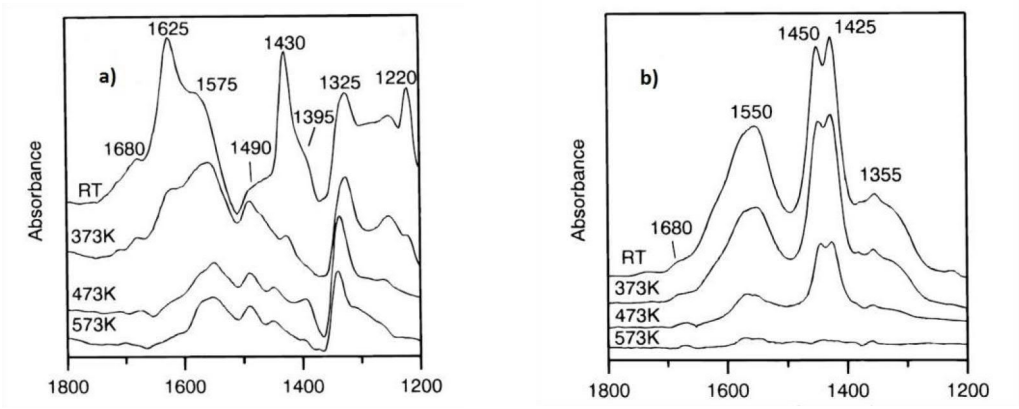


**Figure 14. DRIFTS spectra of $CO_2$ adsorbed on zirconia samples a) monoclinic zirconia b) tetragonal and or cubic zirconia** [25]**.** *(RT: room temperature)*

The surface sites and adsorption of $CO_2$ on the monoclinic zirconia surface can be characterized with DRIFTS experiments [9,10,27,28,62]. $CO_2$ adsorption arises to different structures on the monoclinic zirconia surface, in Figure 15.

Bicarbonates are formed when $CO_2$ reacts with hydroxyl groups on monoclinic zirconia. Monodentate carbonates species are formed when $CO_2$ reacts with $O^{2-}$ centers, bidentate carbonates are formed when $CO_2$ reacts with $Zr^{4+}$–$O^{2-}$ and polydentate carbonates when $CO_2$ reacts with $Zr^{4+}$. These species can be identified with their assigned wavenumbers from the DRIFTS spectra, in Figure 16 [27].

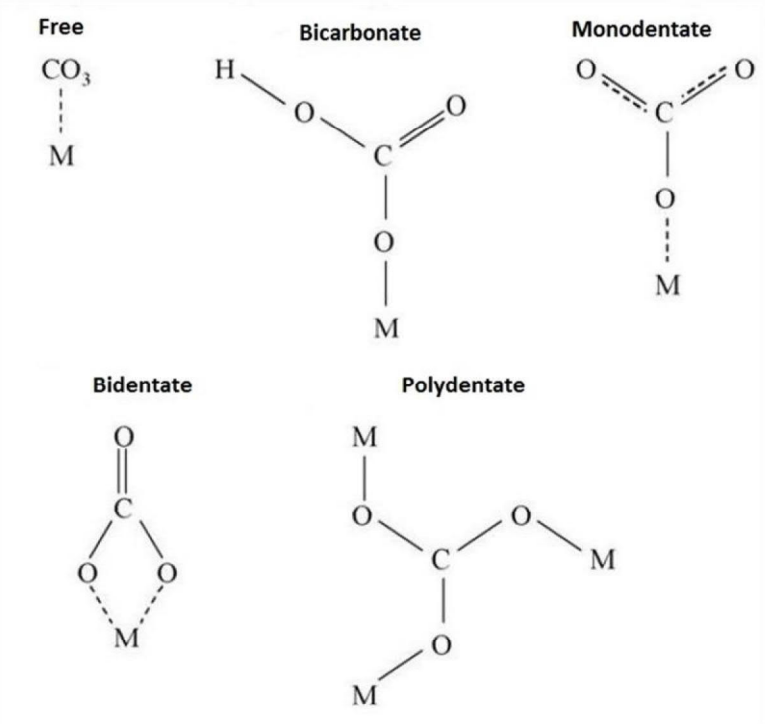


**Figure 15. The surface carbonate species from the adsorbed $CO_2$ on monoclinic zirconia** [27]**.**

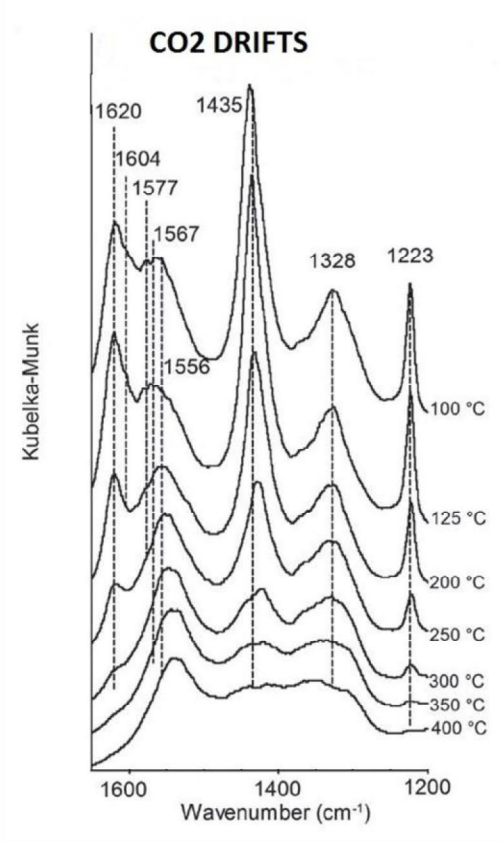


| Wavenumbers | Species |
|---|---|
| 1223 | Bicarbonate |
| 1620 | Bicarbonate |
| 1570-1560 | Bidentate carbonate |
| 1397 | Monodentate carbonate |

**Figure 16. $CO_2$-DRIFTS spectra on monoclinic zirconia with carbonate species and their assigned wavenumbers** [9]**.**

### 2.5.3 Zirconia nanorods

As mentioned earlier, nanostructured catalyst are of great interest due to their ordered pore structure and size, high surface area, framework and surface properties [14,65]. In catalysis, the nanoshapes are beneficial due to their well-defined surface sites, which can linked easily to the selectivity depending on the exposed surfaces [10,15]. These nanostructures can be prepared and controlled depending on the preparation conditions. A high surface area is another requirement for a better catalyst, which allows well-dispersed catalytic phase with high loadings. Taking in account the catalytic reaction occurs on the catalysts surface, high surface area results

improved activity and selectivity. Similarly, $CO_2$ adsorption in nanoporous materials is an energy efficient process and offers separation capability [14].

In particular, nano-sized zirconia have been applied in preparation of oxygen sensors, optical devices, fuel cells, coatings, catalyst support and ceramics [13,66,67]. Fulfilling most of the above-mentioned need for a better catalyst support and adsorption of $CO_2$ as well, monoclinic zirconia nanorods could result an interesting catalyst support.

### 2.5.4 Zirconia nanorods preparation methods

Monoclinic zirconia have been prepared in nanoshapes, nanorods and nanosheets [15,65-75]. $ZrO_2$ nanoparticles have been prepared with various preparation methods as follows:

- Hydrothermal and solvothermal synthesis [13,15,64,66,69,75],
- Sol-gel synthesis [72],
- Aqueous-phase precipitation [73],
- Pyrolysis of Zr–organic precursors [74].

Methods to be employed for the preparation depend on the application requirements. The properties of the compounds can vary with the preparation methods and thus can result in difference on the catalyst activity and surface chemistry. Especially, nanorods/nanobars shaped zirconia have been prepared by hydrothermal synthesis [13,15,64,66,69]. This literature part includes only review of hydrothermal synthesis method.

#### *2.5.4.1 Hydrothermal synthesis*

Hydrothermal synthesis involves formation of product under the action of water at high temperatures and pressures. Hydrothermal conditions are controlled by temperature, pH and redox potential of the environment and the activity of ingredients [76]. It can be based on crystallization in an aqueous solution under increasing pressure and temperature and can be conducted in an autoclave [77]. Hydrothermal

method has been used widely as it yields well-shaped and fine metal oxide particles [64]. Especially, nanorods/nanobars shaped zirconia have been prepared by hydrothermal synthesis [13,15,64,66,69].

Reference [15], presented the preparation procedure of m-$ZrO_2$ via hydrothermal synthesis. In the preparation, $Zr(NO_3)_4.5H_2O$ and NaOL (sodium oleate) are mixed and heated in an autoclave at the pH 9.4 which was monitored with ammonia water. NaOL, the capping agent, was used for the growth of the nanorods shape as explained. The proposed formation route of m-$ZrO_2$ is presented in Figure 17.

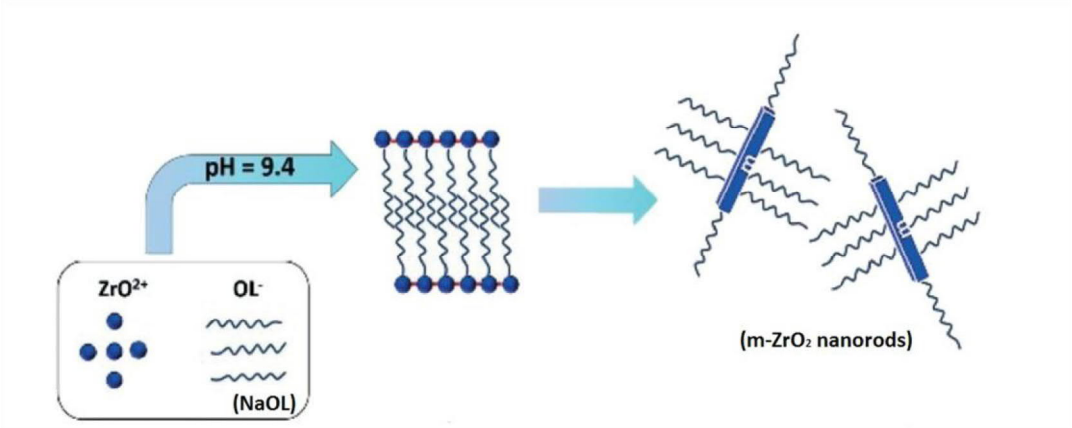


**Figure 17. The formation routes of m-$ZrO_2$ nanorods** [15]**.**

As reported in another reference [69], monoclinic zirconia nanorods were prepared by hydrothermal synthesis. In the preparation procedure, $ZrB_2$ and $H_2O_2$ were used followed by sealing in an autoclave in an elevated temperature. The as synthesized amorphous $ZrO_2$ were later annealed in the air and m-$ZrO_2$ nanorods were obtained. The preparation and formation of m-$ZrO_2$ during the hydrothermal synthesis is presented in Figure 18.

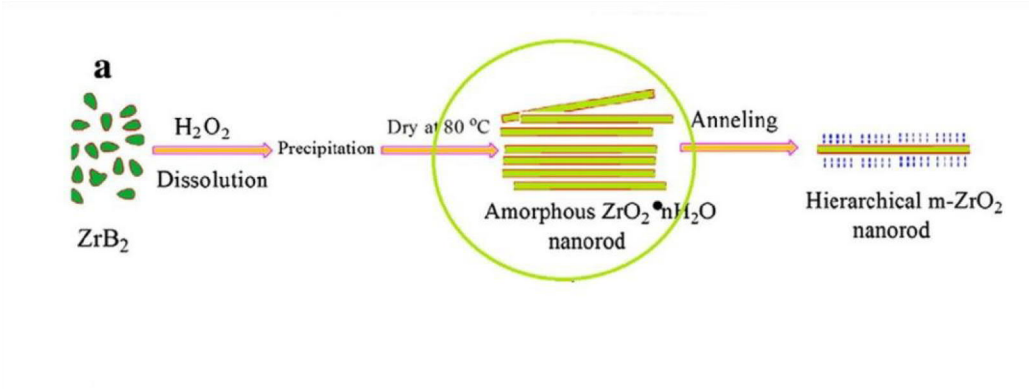


**Figure 18. m-$ZrO_2$ nanorods formation** [69]**.**

### 2.5.5 Supported catalysts

The support and the active component together fulfil the requirement of the catalyst. Support plays a significant role in providing thermal stability, strength and even provides shape to the active component and the activity and selectivity are due to the active component [8,29,49]. The visualization of active component with and without a support is presented in Figure 19. The activity of the solid catalyst is proportional to the active surface area per unit per volume of catalyst. High activity per unit volume can be achieved with smaller particles.

Supported catalyst can be divided in two groups depending upon the nature of the active components: precious/noble metals and base metals. For the supported catalyst with the expensive active component (noble metal), maximum active surface area per unit weight of the active component is preferred whereas, for the base metals, supported catalyst active surface area per unit volume is preferred [29].

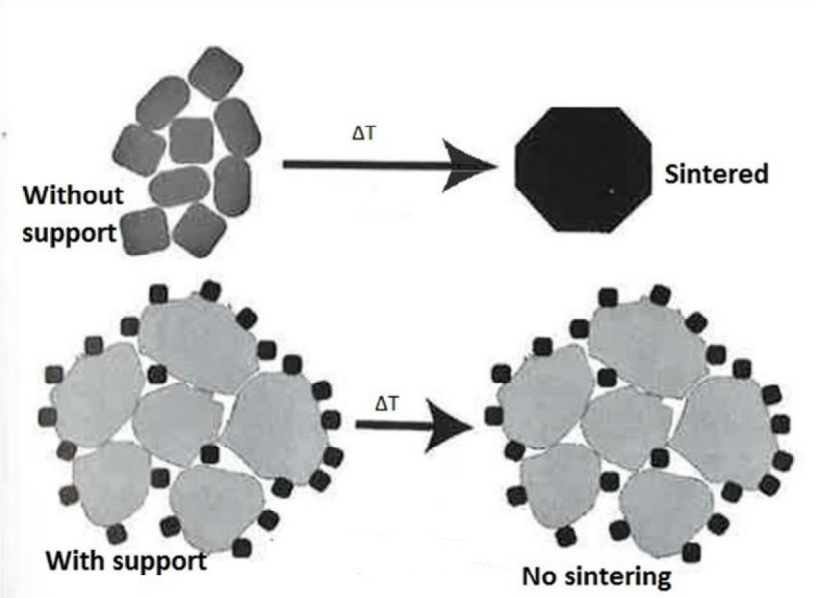


**Figure 19. Active component with and without support material. Modified from the reference** [29]**.**

The particle size, dispersion and surface area of the active component on the support depends on the preparation methods of the supported catalyst [29]. The most common preparation routes of the supported catalyst are as follows:

- Deposition–precipitation [29,31],
- Impregnation and drying [27,30–39,41–45],
- Co-precipitation [32,34,38,40].

Impregnation is one of the most used methods for the noble-based catalyst preparation [27,35,37,39–45]; this review includes details only about the impregnation method in further sub-section.

#### *2.5.5.1 Impregnation and drying*

Impregnation can be simplified as method that involves bringing the precursor solution into the pores of the support. The simplest way to execute impregnation is putting the volume of the precursor solution same as the pore volume of the dried support and the solution is drawn into the pores by capillary action. The liquid penetration in the pores requires elimination of the air from the pores of the support. But the part of the air present in the pore space can be remain as bubbles and compressed due to the capillary forces. The forces will be exerted on the pore walls in contact with these bubbles and can result in bursting of the grains. This can be reduced by impregnation under vacuum as being highly compressed air dissolves and escapes progressively from the support surface. After impregnation, there needs elimination of the solvent (water). The catalyst is heated up to the boiling point of solvent or very gentle drying is carried out at low temperature. The elimination of water from the pores leads to the increase in concentration of the precursor on the support and results high dispersion. [29, 78]

# 3 EXPERIMENTAL SECTION

## 3.1 Materials

The list of materials used for the catalyst preparation is presented in Table 3 with their specifications. All the aqueous solutions were prepared using MilliQ water obtained from water purification system (Millipore Synergy).

**Table 3. List of the materials used for catalysts preparation.**

| Materials | Specifications |
|---|---|
| Zirconium(IV)nitrate | $Zr(NO)_3)_4.5H_2O$ (≥ 99,99 %, BOC Science) |
| Sodium Oleate (NaOL) | $C_{18}H_{33}NaO_2$ (≥ 99 %, Sigma-Aldrich) |
| Ammonium hydroxide | $NH_4OH$ (28% $NH_3$ in $H_2O$, ≥ 99,99 %, Sigma-Aldrich) |
| Ethanol | $C_2H_5OH$ (≥ 99,5 %, ALTIA Oyj) |
| Cyclohexane | $C_6H_{12}$ (anhydrous, ≥ 99,5 %, Sigma-Aldrich) |
| Monoclinic zirconia | $ZrO_2$ pellets (≥ 99,5 %, Saint Gobain) |
| Rhodium(III)nitrate | $Rh(NO_3)_3$ (10% (w/w) (Rh in >5 wt% $HNO_3$), Sigma-Aldrich) |

## 3.2 Catalysts Preparation

Two different zirconia supports, namely monoclinic zirconia nanorods and the commercial monoclinic zirconia were the supports used for Rhodium (Rh) through-out this thesis. In the text and figures, these supports will be abbreviated as $ZrO_2$ NRs and com $ZrO_2$ respectively. $ZrO_2$ NRs was prepared via *hydrothermal synthesis* method whereas the com $ZrO_2$ was purchased. Rh was loaded by wet impregnation on both the supports. This chapter will describe the preparation procedure of the catalysts distinctly in two phases: the support preparation and the metal loading.

### 3.2.1 Synthesis of monoclinic zirconia nanorods

#### *3.2.1.1 Hydrothermal synthesis*

During the preparation, 32.8 ml of $Zr(NO)_3)_4.5H_2O$ (0.117 mol/L) aqueous solution was mixed with 16.4 ml of NaOL (0.233 mol/L) aqueous solution and the white precipitate was formed under stirring at room temperature, with [Zr]/[NaOL] molar ratio of 1/1. 1.1 ml of $NH_4OH$ solution was added in the mixture and after adding 37.2ml of water, the mixture was transferred to 125 ml autoclave (acid digestion vessel 4788, Parr) at pH 9. The autoclave was kept in the oven (Memmert oven) heated to 200 °C with the ramp of 5 °C per minute and kept for 20 h at that temperature. The preparation procedure was modified from the reference [15].

#### *3.2.1.2 Centrifugation and washing*

The slurry was transferred to the 50 ml glass centrifuge tubes and placed in the centrifuge (Multifuge 3S, Heraeus, Kendro Lab Instruments) at 4000 rpm to separate the precipitate from aqueous slurry. The precipitate was washed thoroughly with, ethanol and cyclohexane-ethanol mixture where 10 vol% of cyclohexane was used, to remove the oleate. After washing, the precipitate was left for drying at 80 °C overnight and the crystals were ground and stored in ambient temperature.

#### *3.2.1.3 UV-ozone treatment*

UV-ozone treatment was carried out in UV-ozone cleaner (PSD Pro Series, NovaScan) equipped with mercury vapor lamps. The equipment produces a high output UV radiation from the lamps emitting mercury vapor at the distance of 5 cm. The UV radiation is produced by the lamps at wavelengths of 250 nm and 180 nm; in turn the radiations produce highly reactive ozone from the external oxygen supplied in the chamber. The reactive ozone interacts at the molecular level with contaminants (oleate in this case) causing them to decay. The treatment was performed in pure oxygen atmosphere.

$ZrO_2$ NRs crystals were ground and put in the flat aluminum foil. The foil was placed in the chamber of UV ozone cleaner at the distance of 5 cm from the lamp. 5

NL/min $O_2$ was let to flow in the chamber for 10 minutes and the UV-ozone cleaner was left on with timer. At the interval of 3 hours, the sample was taken out, weighed and the weight loss percentage was recorded. Sample was gently shaken for homogenous distribution in the foil and to ensure the sample exposure to UV radiation during the treatment.

*3.2.1.4 Palletization and sieving*

UV treated $ZrO_2$ NRs was pelletized with hydrostatic pressurization using High Pressure Multivessel Apparatus U111. The Multivessel apparatus had two chambers (vessels) of volume 8ml and 13 mm diameter with propylene glycol as the pressure medium.

(200-300) mg of $ZrO_2$ NRs was sealed in silicone tubing (ϕ 10 mm) and placed into the chamber of multivessel apparatus filled with Millipore water. The chamber was closed and a pressure around 1000 bars was applied to the chamber via hydraulic oil pump for 2 minutes. The $ZrO_2$ NRs pellets were ground and sieved to 250–420 µm particles. The purchased com $ZrO_2$ was in rod-shaped pellets which was ground and sieved to 250–420 µm particles as well.

*3.2.1.5 Calcination*

Prior to the metal loading the sieved supports, $ZrO_2$ NRs and com $ZrO_2$ (250–420 µm), were calcined at 350 °C for 2 hours under air flow of 75ml/min (20 vol% $O_2$ and 80 vol% $N_2$), schematically shown in Figure 20.

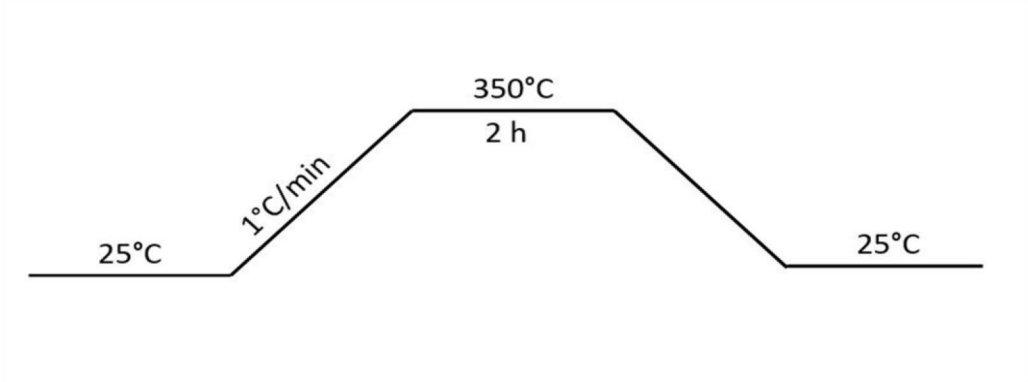


**Figure 20. Temperature profile of calcination.**

### 3.2.2 Rhodium loading

Catalysts, Rh/$ZrO_2$ NRs and Rh/com $ZrO_2$ were prepared by vacuum wet impregnation using $Rh(NO_3)_3$ solution as a precursor. Two batches with each support, $ZrO_2$ NRs and com $ZrO_2$, were prepared with the targeted Rh loadings 0.5 wt% and 2 wt%.

The desired amount of support was taken in a two-neck round bottom flask and dried in vacuum under water bath at 90–95 °C for an hour. Vacuum was retained in the bottle and let it cool down. The required amount of precursor solution and water was taken and mixed. The precursor solution was injected to the support in vacuum through a septum using short-needled syringe (FINE JECT 0.45X12 mm needle, 1 ml syringe). The catalyst was swirled for an hour and left overnight to settle. Then, the catalyst was dried rotating the flask in vacuum under water bath at 40 °C for 1.5 h and at 60 °C for 30 minutes. The catalysts were in-situ calcined during the reaction at 350 °C. Figure 21 illustrates the set-up for wet impregnation.

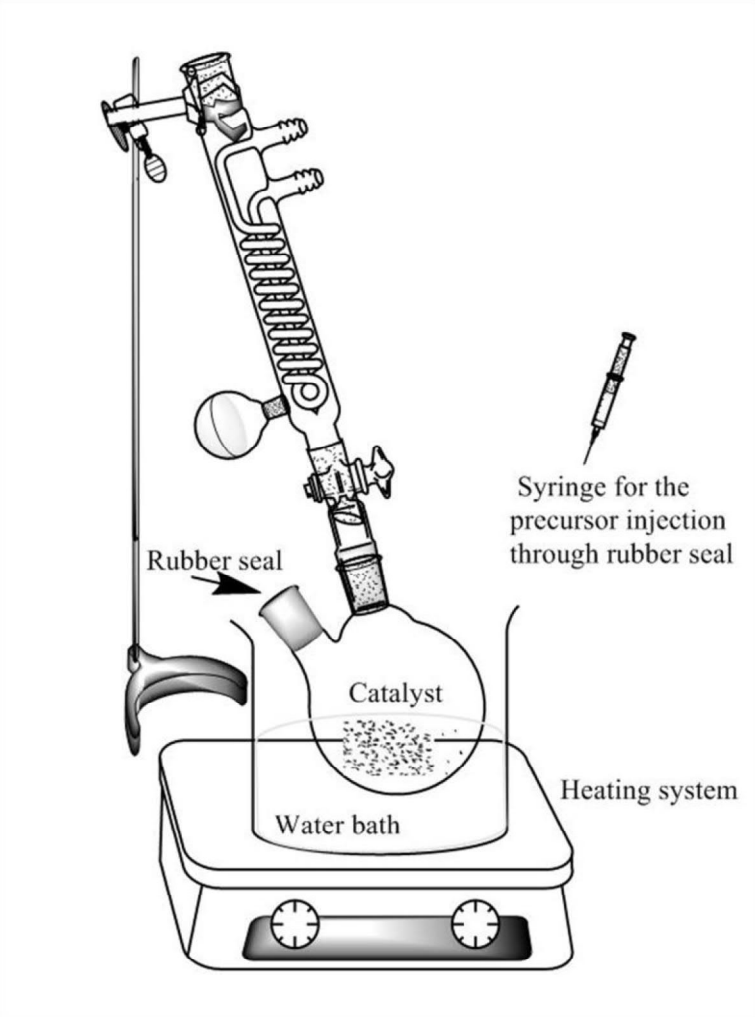


**Figure 21. Set-up for the wet impregnation of the precursor on the support.**

Table 4 includes the prepared catalysts and their abbreviated names, which will be further used in text and figures.

**Table 4. Catalysts prepared with different metal loadings and supports.**

| Supports | Targeted Rh loadings (%) | Catalysts designation |
|---|---|---|
| $ZrO_2$ NRs | 0.5 | 0.5Rh/$ZrO_2$ NRs |
| $ZrO_2$ NRs | 2 | 2Rh/$ZrO_2$ NRs |
| com $ZrO_2$ | 0.5 | 0.5Rh/com $ZrO_2$ |
| com $ZrO_2$ | 2 | 2Rh/com $ZrO_2$ |

## 3.3 Catalysts characterization

***Transmission-electron microscopy***

Transmission-electron microscopy imaging (TEM) (JOEL JEM-2200FS operated at 220kV) was performed to obtain the information on the shape of prepared zirconia support as well as the dimensions. The images were obtained with the resolution of 20 nm and the dimensions were measured using TEM-imaging software.

***X-ray photoelectron spectroscopy***

X-ray photoelectron spectroscopy (XPS) measurement was carried out to analyse the chemical compositions and characterize the oleate on $ZrO_2$ NRs surface. AXIS Ultra spectrometer was used for the analysis with monochromatic Al Kα radiation at 100 W, under neutralization. The known peak positions from the cellulose was used to deconvolute C–region; adjusting binding energy of C 1*s* peak to 285 eV. UV–ozone treated samples for two different time intervals, 15 h and 21 h were chosen for the XPS analysis.

***In situ reflectance Fourier transform infrared spectroscopy***

The types and evolution of OH groups and $CO_2$ adsorption on zirconia supports were studied by *in situ* diffuse reflectance Fourier transform infrared spectroscopy (DRIFTS). The measurements were carried out with an infrared spectrometer (Nicolet, Nexus FTIR) and chamber (Spectra-Tech), ZnSe as a window material. The total gas feed was 50 ml $min^{-1}$ and the flow rates and compositions of gases were monitored on-line with a mass spectrometer (Pfeiffer Vacuum Omnistar). The background spectrum was recorded using aluminium mirror under nitrogen flow where 400 scans were taken for wave numbers from 600 $cm^{-1}$ to 4000 $cm^{-1}$ at the resolution of 4 $cm^{-1}$. The ground sample (zirconia support) was in situ calcined with 5 vol% $O_2/N_2$ at 350 °C for 2h. After cooling down to 30 °C, 10 vol% $CO_2/N_2$ was let in the sample chamber for 30 minutes and the spectra of the sample were recorded every 5 minutes. After the $CO_2$ flow, the sample was flushed with nitrogen for 30 minutes

and the spectra were recorded again every 5 minutes. During the measurements, 100 scans were taken for each spectrum for wave numbers from 600 $cm^{-1}$ to 4000 $cm^{-1}$ with a resolution of 4 $cm^{-1}$. The scheme of In situ DRIFTS experiment with the gas feed, time and temperature is schematically presented in Figure 22.

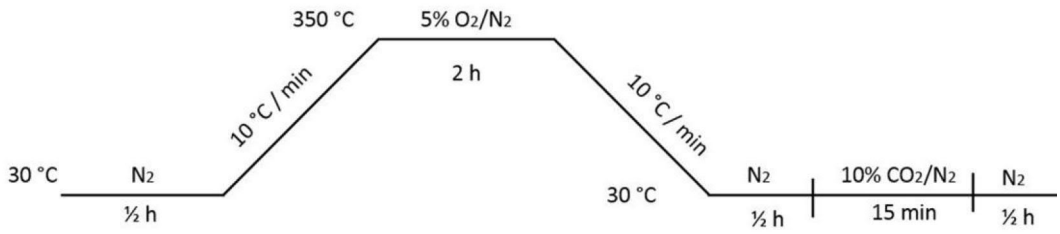


**Figure 22. Reaction scheme in the DRIFTS experiments.**

***X-ray Diffraction***

The phase of the prepared $ZrO_2$ NRs was analyzed by X-ray diffraction (XRD). XRD patterns were collected in 2θ range from 15 ° to 70 ° with PANanalytical X'pert Pro diffractometer using Co Kα-1 radiation (1.789Å), operating at 40 kV and 40 mA. The diffraction angle (2θ) calculation is based on Bragg's law of diffraction given in equation 5 [2].

$$\boldsymbol{n\lambda = 2d\,sin\theta} \qquad (5)$$

where,

λ is wavelength of the X-ray,

θ is the diffraction angle,

d is lattice spacing and

n is a positive integer, also called order of reflection.

***Nitrogen physisorption***

Thermoscientific's SURFER instrument was used for obtaining the $N_2$ adsorption-desorption isotherms under nitrogen flow at -176 °C. 200 mg of sample was used for the experiment and the sample was outgassed at 150 °C for 5h prior to $N_2$ adsorption. The pore volumes were calculated according to the Gurvich method for p/p° =0.99 and the Barrett-Joyner-Halenda (BJH method) whereas, the total surface area of the catalysts was obtained from Branauer-Emmert-Teller (BET) [51,84-86]. The pore volumes and surface area was calculated using Advanced Data Processing software, following the isotherms.

***$H_2$ chemisorption***

Thermoscientific's SURFER instrument was used for obtaining the $H_2$ adsorption isotherms at room temperature. 100–200 mg of samples were loaded in burette, started with reduction in $H_2$ at 350 °C for 2 h and then the samples were evacuated at 350 °C for 2 h. The $H_2$ adsorption isotherms were recorded and a subtraction isotherm was obtained to calculate the irreversible $H_2$ volume. Then, the amount of monolayer volume, dispersion and mean particle diameter was calculated using Advanced Data Processing software following the isotherms.

***X-ray fluorescence***

Rhodium loadings on $ZrO_2$ NRs and com. $ZrO_2$ supports was measured by X-ray Fluorescence (XRF) spectrometer ($AXIOS^{mAX}$, PANanalytical). The instrument, $AXIOS^{mAX}$, configuration had Rh-anode or X-ray source with tube voltage 60Kv and the brass filter (400µm).

***Thermogravimetric analysis***

Thermogravimetric analysis (TGA) was carried using TA Instruments Q500 Thermogravimetric Analyzer to determine the decomposition temperature of Rh precursor for the catalyst calcination. Non-calcined catalyst after metal loading, 0.5Rh/com $ZrO_2$, was analysed by TGA where the sample (42.6 mg) was heated from room temperature to 600 °C in nitrogen with the heating rate of 5 °C/min.

## 3.4 Catalysts testing: $CO_2$ hydrogenation

### 3.4.1 Testing set-up

***Temperature-programmed catalyst characterization instrument***

During this thesis work, (Altamira Instruments) AMI-200R catalyst characterization instrument equipped with Thermal Conductive Detector (TCD) was used for the catalytic reaction. The instrument was equipped with gas feeds to perform the reactions. The auxiliary vent in the instrument allows to route the reactant gases to another detection device directly (eg. GC or MS). In this work, the gases were withdrawn from analytical vent via a gas tight syringe (SGE, 5ml glass syringe) and taken to GC for the analysis. A complete overview of the scheme in AMI-200R and the gas syringe connection set up is shown in Figures 23 and 24 respectively.

The catalytic reactions were performed in the fixed bed U-tubes reactors with quartz wool on the bottom and top of the catalyst bed. The reactor was heated using oven with temperature controller and the testing set-up is shown in Figure 25. The gases used during the reactions were supplied by AGA with 99.99% purity.

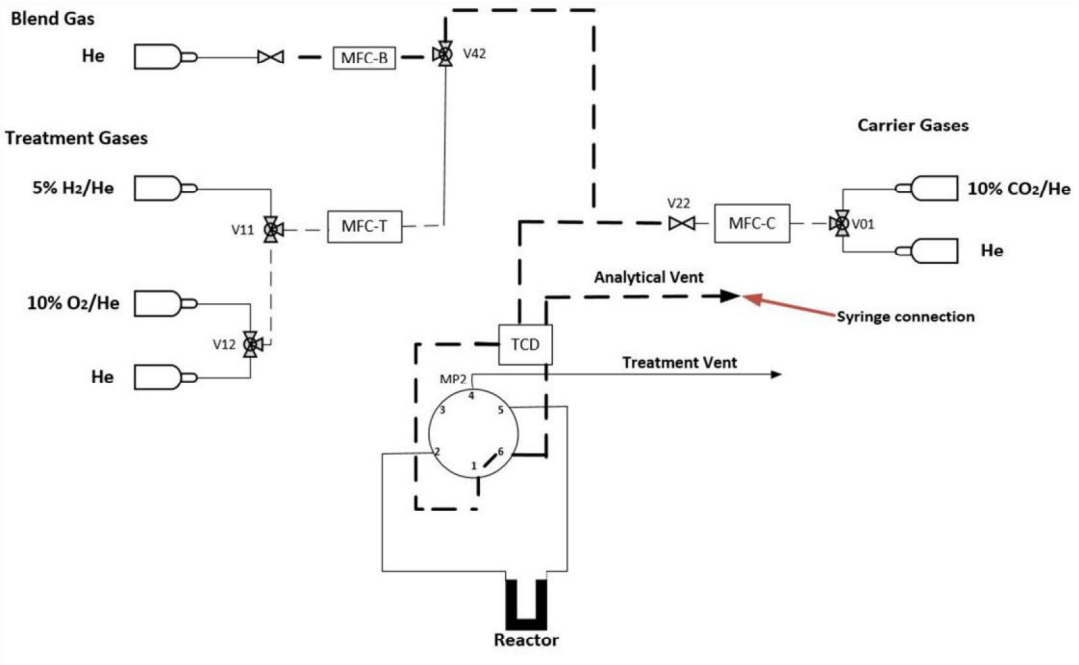


**Figure 23. The scheme from AMI-200R instrument.**

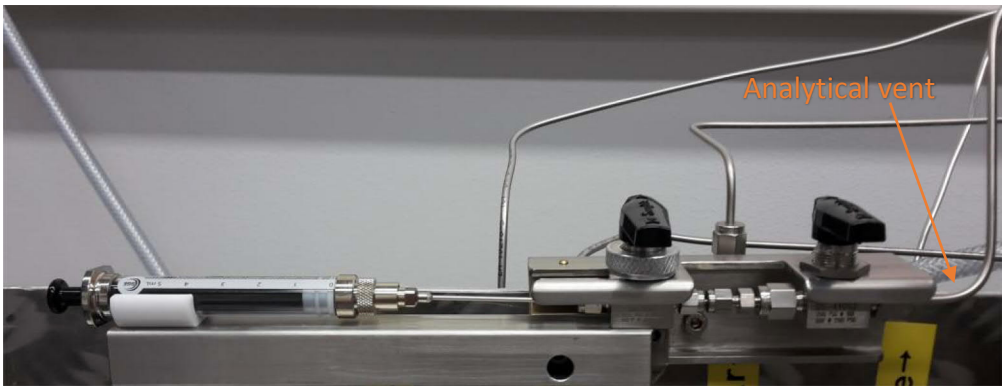


**Figure 24. Syringe set-up for the product gases withdrawal, connected to the analytical vent of AMI-200R set-up.**

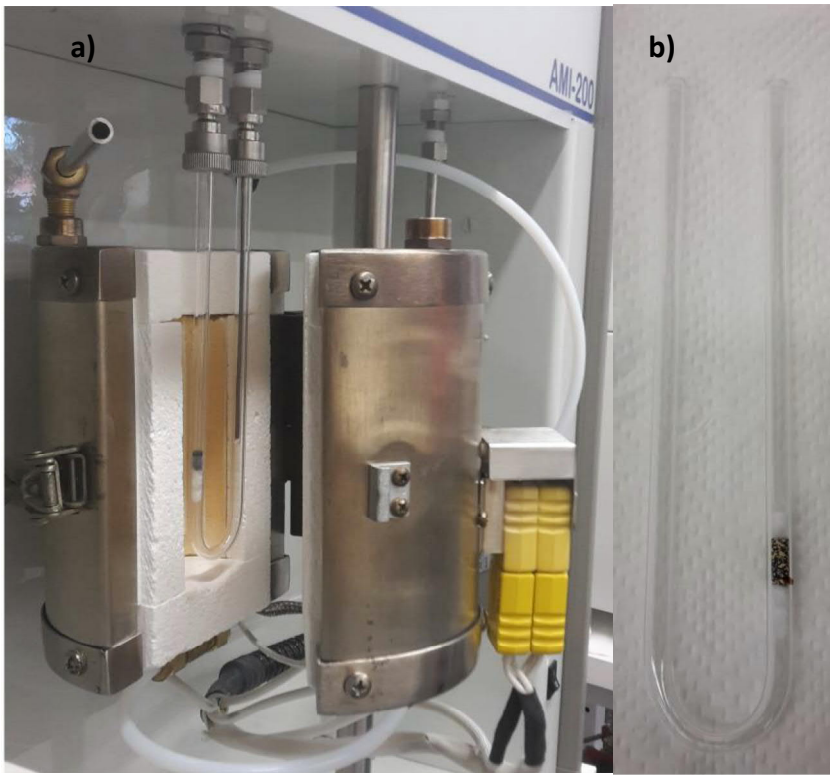


**Figure 25. a) Reactor set-up in AMI-200R b) U-tube reactor with catalyst.**

***Gas Chromatography***

Gas Chromatography analysis was carried out with Agilent 6890N Network Gas Chromatograph. The chromatograph was equipped with two detectors namely; Flame Ionization Detector and Thermal conductivity Detector which will abbreviated as FID and TCD respectively in the texts and pictures. The GC was calibrated with AGA Oy Ab calibration gas mixture before analysis.

CO, $CO_2$, $H_2$ and $N_2$ gases were analysed with TCD connected to two columns: HP-PLOT/Q (30 m x 0.53 mm x 40 µm) and Mole sieve (30 m x 0.53 mm x 25 µm). Hydrocarbons were detected with FID connected to column $Al_2O_3$/KCl (50 m x 0.32 mm x 8 µm). The heating program started from 40 °C with 9.5 min hold time to 200 °C and the heating rate was 10 °C/ min.

### 3.4.2 Reaction tests

As already mentioned, the $CO_2$ hydrogenation was set to carry out in the U-tube reactor where the pressure drop and mass transfer problem would arise. The problem of mass transfer limitations is often observed in the heterogeneous catalysts, which could be the limiting factor to observe the activity of the catalysts. Adjusting the particle size of the catalyst and the relative velocity of the gas could overcome the mass transfer limitations in heterogeneous catalysts [87]. Keeping the conversion level lower allows to observe the rate of change (kinetics) during the reaction and the activity of the catalyst could be studied. Conversion level was adjusted by changing the flow of the reactant gases and amount of the catalysts during the reaction. The catalyst prepared with 0.5Rh/com $ZrO_2$ was tested with different flows and amount of catalysts. On the basis of the results, the flow and amount of the catalysts to be used further for tests was decided; which would be further discussed in the Section 4.3.

This section describes about reaction conditions, the amount of catalysts used during the reaction and the product analysis done in $CO_2$ hydrogenation.

***$CO_2$ and $H_2$ reaction***

The performance of the catalysts was evaluated for the gas-phase carbon dioxide hydrogenation to methane. The reactions were performed in AMI-200R, using U-tube fixed bed reactor, at atmospheric pressure. A programme was defined using AMI-200 software where the reaction steps, temperatures, flow of the gases and time were specified, schematically presented in Figure 26. Catalyst was loaded in the U-tube reactor and the programme was scheduled to run.

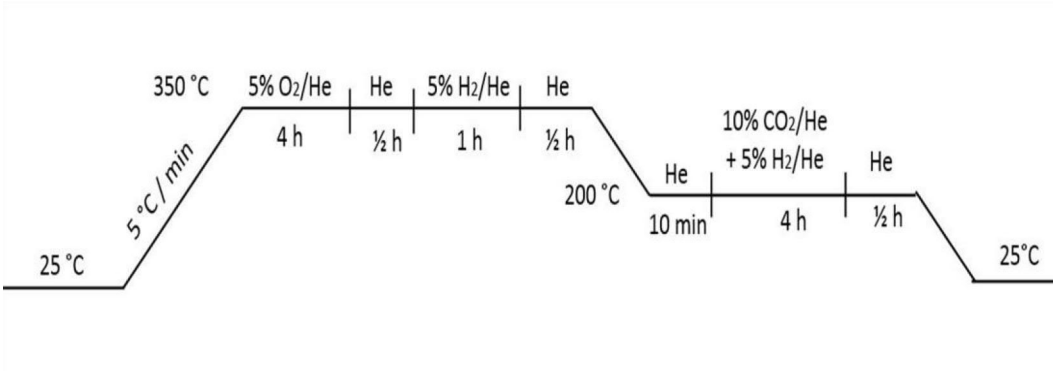


**Figure 26. Reaction profile in AMI.**

The catalyst was in situ calcined using 25 ml/min flow of 5 vol% $O_2$/ 95 vol% He for 4 h and reduced using 25 ml/min flow of 10 vol% $H_2$/ 90 vol% He for 1 h, both at 350 °C. The gas mixture of 10 vol% $CO_2$/ 90 vol% He and 5 vol% $H_2$/ 95 vol% He was feed during the $CO_2$ hydrogenation reaction. The total feed flow was 25 ml/min where the volume percentage of $CO_2$ and $H_2$ was 2, and pure Helium was used as blend gas. The reaction was carried out for 4 h with WHSV 1500 $h^{-1}$ to 6000 $h^{-1}$ at 200 °C. The mass of the catalysts used was 0.2 g in all the reactions and the catalyst was diluted with SiC for higher loadings of Rh given in Table 5.

The product gases were drawn in the gas tight syringe at the interval of each half an hour during the 4 h carbon dioxide hydrogenation reaction. The syringe was quickly transferred to gas chromatography and injected for the analysis.

**Table 5. Amount of catalysts used during the tests.**

| Wt. of Rh in the catalysts (%) | Amount of catalysts used (g) | SiC (g) |
|---|---|---|
| 0.5 | 0.2 | - |
| 2 | 0.05 | 1.5 |

***Product analysis and calculations***

The reactant and product gases were analysed by Gas Chromatography (Agilent 6890N) with ChemStation offline software. The conversion of $CO_2$ was calculated based on mole percentage of $CO_2$ that formed carbon-containing products using the equation 6.

$$Conversion\ (\%) = \frac{\sum n_i \ * \ m_i}{m_{CO2}} * 100 \qquad (6)$$

The selectivity to product *i* was calculated based on the total number of carbon atoms in the products using equation 7.

$$Selectivity\ (\%) = \frac{n_i \ * m_i}{\sum n_i \ * \ m_i} * 100 \qquad (7)$$

In above mentioned equations 6 & 7, $n_i$ is the number of carbon atoms in product *i*, $m_i$ is the mole percent of product *i* detected and $m_{CO2}$ is the mole percent of $CO_2$ in the feed.

Products yield (Y) was calculated using total conversion and selectivity of each product using equation 8.

$$Y\ (\%) = Conversion * selectivity\ of\ product\ i \qquad (8)$$

Weight hourly space velocity (WHSV) was calculated using total flow of reagent ($CO_2$) in the reactor per hour and amount of catalyst, given in equation 9.

$$WHSV = \frac{reagent\ CO_2\ (cm^3)}{h} * \frac{1}{catalyst\ (g)} \qquad (9)$$

Turn over frequency (TOF) was calculated using number of moles of product per mass of catalyst per time, given in equation 10.

$$TOF = \frac{moles\ of\ product\ (CH_4\ )}{moles\ of\ Rh\ in\ catalyst * time\ (h)} \quad (10)$$

# 4 RESULTS

## 4.1 Zirconia nanorods yields

### 4.1.1 Batches yields after centrifugation and washing

7 batches of $ZrO_2$ NRs were synthesized, following the preparation procedure and compositions mentioned in Section 3.2.1 and total yield was 2.56 g. Yields from each batch is given in Table 6. From the table, some batches resulted less yields which could be due to effective removal of oleate after washing with ethanol and cyclohexane. The time and amount of washing solvent could be increased for effective removal of oleate and to obtain clean samples.

**Table 6. $ZrO_2$ NRs yields from each batch via hydrothermal synthesis.**

| Batch number | Theoritical yields (g) | Experimental yields (g) | Experimental yields (%) |
|---|---|---|---|
| 1 | 0.47 | 0.399 | **84.6** |
| 2 | 0.47 | 0.372 | **78.8** |
| 3 | 0.47 | 0.352 | **74.6** |
| 4 | 0.47 | 0.386 | **81.8** |
| 5 | 0.47 | 0.337 | **71.4** |
| 6 | 0.47 | 0.324 | **68.7** |
| 7 | 0.47 | 0.397 | **84.2** |
| | | **average ±stdv** | **77.7 ± 5.8** |

### 4.1.2 UV-ozone treatment

After 30 h of treatment for every batch, in an average of 30% weight loss was observed, with no further loss in sample weight indicating the removal of oleate, pre-

sented in Figure 27. The pictures collected for ZrO2 NRs crystals, the color change of the sample before and after UV-ozone treatment are presented in Figure 28.

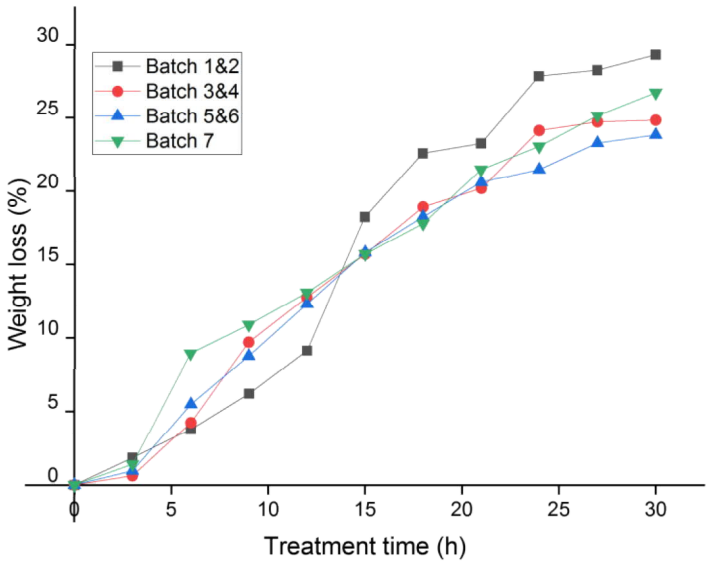


**Figure 27. Weight loss from the batches during UV-ozone treatment.**

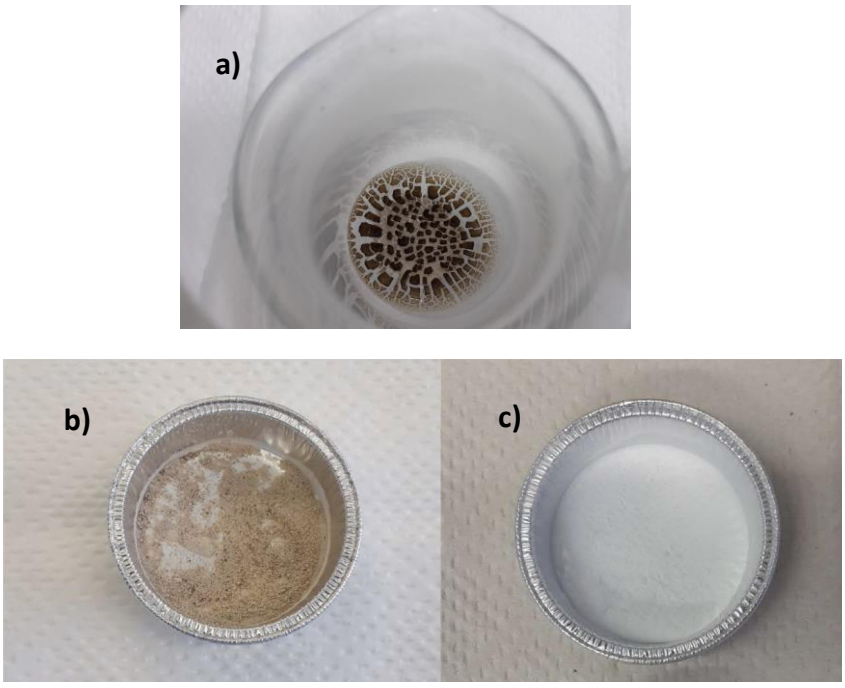


**Figure 28. Sample pictures a) $ZrO_2$ NRs crystals obtained after drying b) Before UV-ozone treatment [as prepared] c) After UV-ozone treatment.**

## 4.2 Characterization Results

### 4.2.1 Support structure and surface

***Transmission-electron microscopy***

The zirconia crystals obtained from the first batch preparation was characterized with TEM. TEM images showed the prepared $ZrO_2$ crystals were nanorods with diameter of 2 nm and 10 nm in length, in Figure 29. TEM images verified the prepared $ZrO_2$ support was nanorods in structure agreeing with the reference [15], so the same preparation procedure was followed for the further batches preparation.

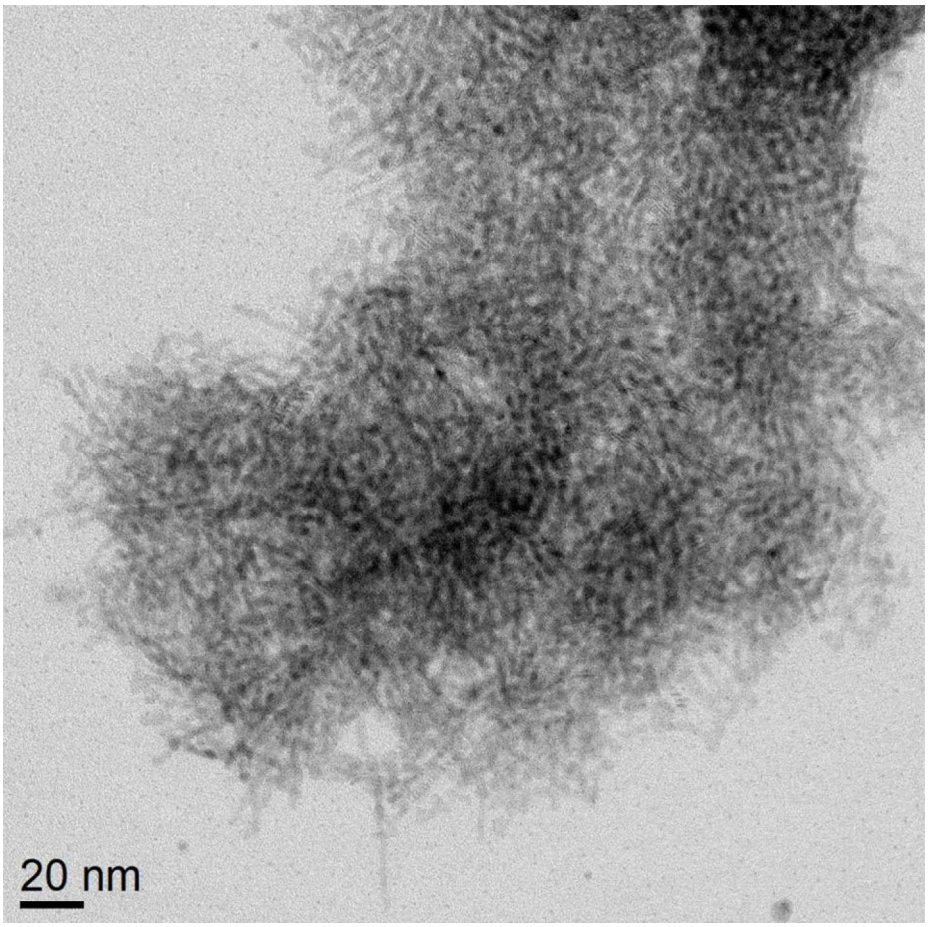


**Figure 29. Zirconia nanorods observed under TEM.**

***X-ray photoelectron spectroscopy***

XPS measurements were performed on the UV-ozone treated samples for 15 h and 21 h, presented in Figure 30. From the results, the Zr position is on the oxidized region as expected. The known peak positions from the cellulose was used to deconvolute C–region; adjusting binding energy of C 1*s* peak to 285 eV. The 15 h treated sample has more carbon with most of the excess in the aliphatic C peak at 285 eV. There is also a change in the ratio of the O 1s peaks after the 21 h treatment that suggests loss of intensity from the higher BE peak, which is associated with organic compounds.

The elemental concentrations analyzed by XPS measurements is presented in Table 7. The results indicate that the sodium oleate amount decreased with the prolonged UV- treatment, but with the observation of carbon confirms that it was not

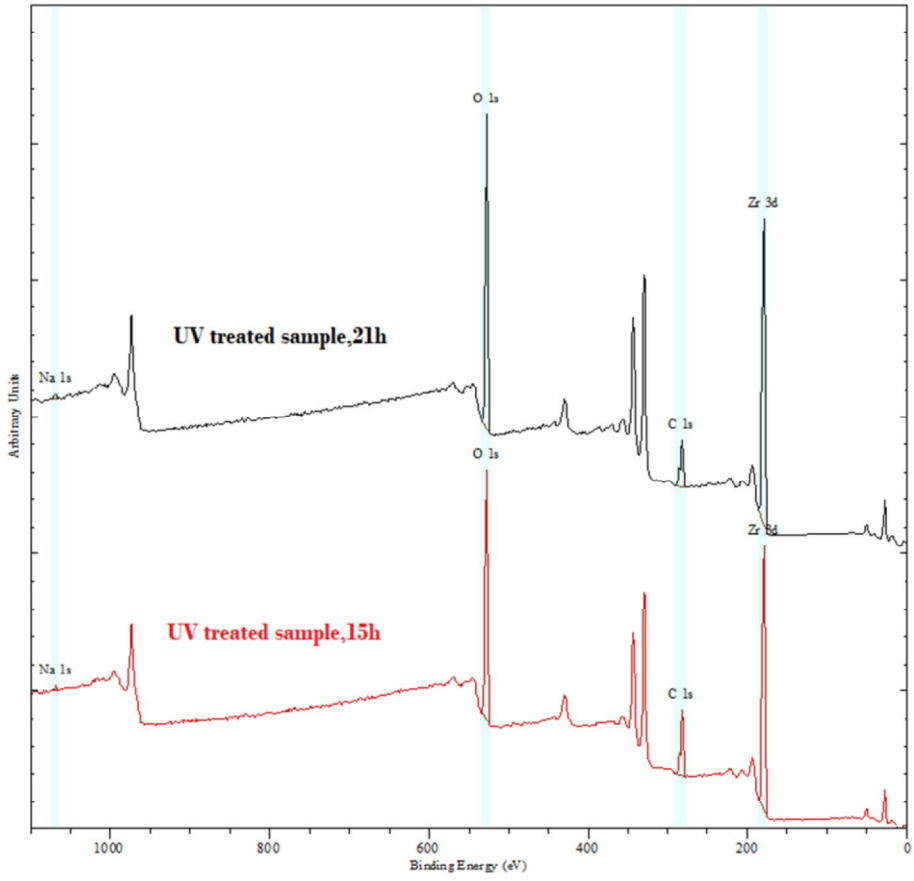


**Figure 30. XPS spectra of $ZrO_2$ NRs support after UV-ozone treatment.**

completely removed. The sample samples were further treated until 30 h and the oleate was characterized with In-situ DRIFTS which will be discussed in following pages.

**Table 7. Elemental concentrations determined from XPS analysis for $ZrO_2$ NRs after 15 h and 21 h of UV-ozone treatment.**

| | BE positions (eV) | Concentration (%) | |
|---|---|---|---|
| | | 15 h | 21 h |
| O 1s | 530.2 | 28.7 | 31.1 |
| O 1s | 532.025 | 17.8 | 18.3 |
| CC | 285 | 20.2 | 14.9 |
| CO | 286.51 | 3.8 | 3.8 |
| OCO | 288.41 | 5.1 | 4.8 |
| COO | 289.3 | 3.26 | 3.1 |
| Zr $3d_{5/2}$ | 182.235 | 12.3 | 13.6 |
| Zr $3d_{3/2}$ | 184.58 | 8.8 | 10.1 |

***In situ reflectance Fourier transform infrared spectroscopy***

DRIFTS experiments were carried out to characterize the surfaces of supports, evolution of hydroxyl groups and $CO_2$ adsorption on their surfaces. The collected spectra for the two supports are compared for the same experimental condition (under $N_2$ or $CO_2$ flow) at room temperature (30 °C).

The spectra collected for as prepared $ZrO_2$ NRs and after calcination of $ZrO_2$ NRs are compared in Figure 31. Sodium oleate bands were observed on the surface of the as prepared $ZrO_2$ NRs at 3000-2800 $cm^{-1}$ and 1600-1400 $cm^{-1}$ indicating the oleate was not completely removed from the surface [88]. After calcination, the bands decreased at the region 3000-2800 $cm^{-1}$ whereas dominant oleate bands appeared at 1600-1400 $cm^{-1}$. The IR bands of hydroxyl sites were observed at 3680 $cm^{-1}$ and 3760 $cm^{-1}$ assigned as tri-bridged and terminal hydroxyl groups respectively [10,27].

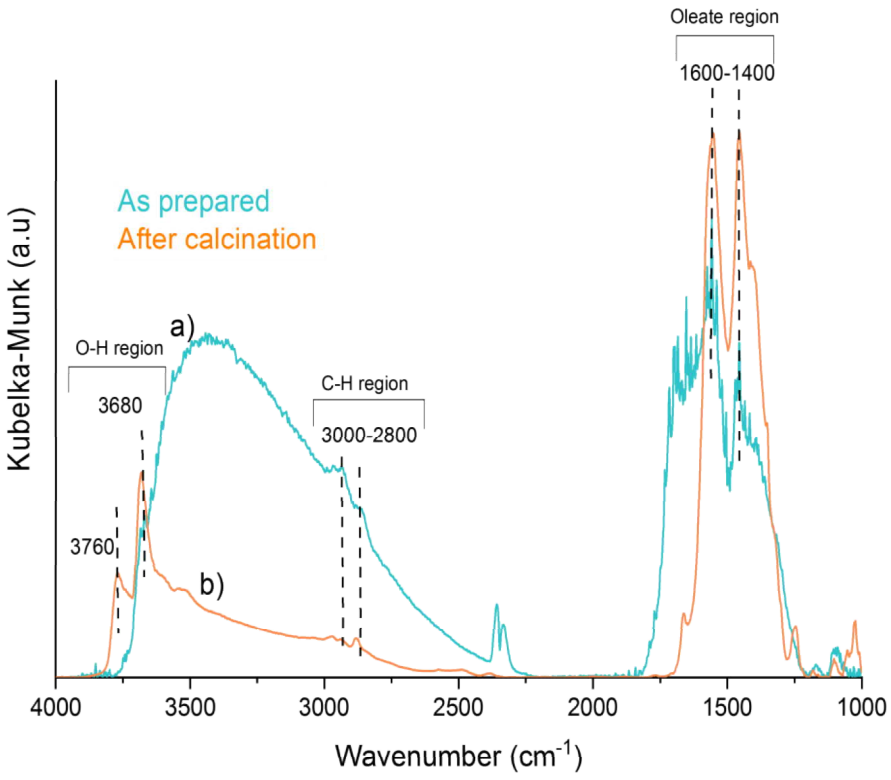


**Figure 31. DRIFTS spectra of $ZrO_2$ NRs at 30 °C a) As prepared b) After calcination at 350 °C.**

Figure 32 presents the comparison of the spectra collected after calcination and after $CO_2$ adsorption on $ZrO_2$ NRs support. It can be seen from the Figure 30, the surface hydroxyl species (terminal hydroxyl) at the band 3760 $cm^{-1}$ decreased with $CO_2$ adsorption, bicarbonates species appeared at 3615 $cm^{-1}$ , linear CO at 2300 $cm^{-1}$ and different structured carbonates at 1600-1400 $cm^{-1}$ [9,10]. It indicates the adsorption of $CO_2$ occurs on the surface hydroxyl sites and involves in the formation of bicarbonates and carbonates species.

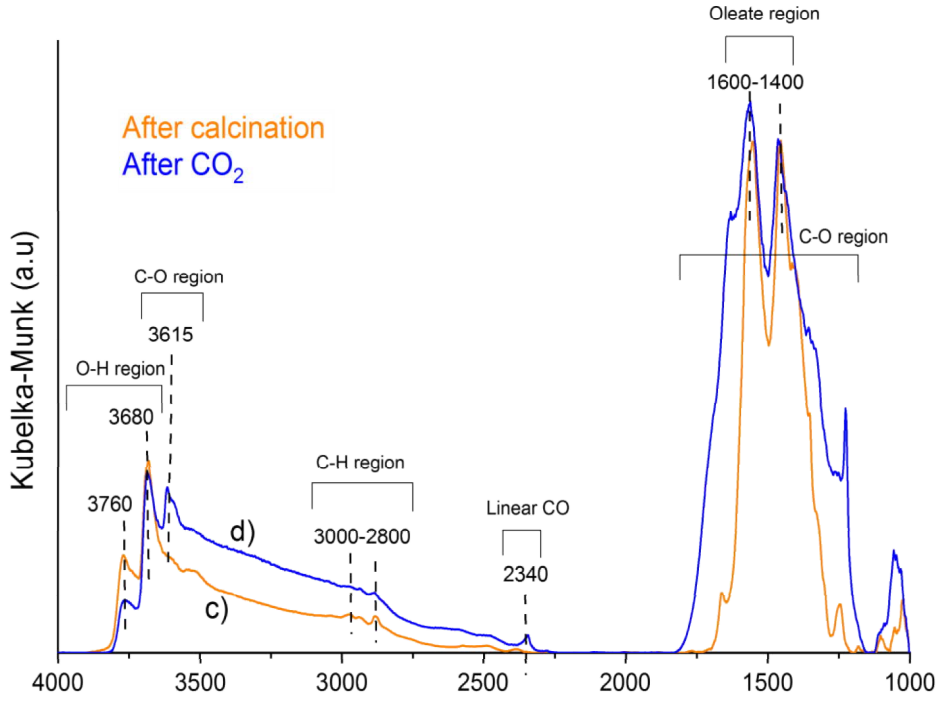


**Figure 32. DRIFTS spectra of $ZrO_2$ NRs at 30 °C. c) After calcination d) After $CO_2$ adsorption.**

Although the IR band appeared boarder after $CO_2$ adsorption, the oleate bands at 1600-1400 $cm^{-1}$ remain dominant. It was therefore difficult to identify the types and intensities of the carbon species formed on the support after $CO_2$ adsorption. The DRIFT subtraction spectra (the spectrum after calcination subtracted from the $CO_2$ adsorption spectrum) was obtained to identify and quantify the adsorbed $CO_2$ species on the $ZrO_2$ NRs, presented in Figure 33 and the names of identified species and their IR wavenumbers in Table 8.

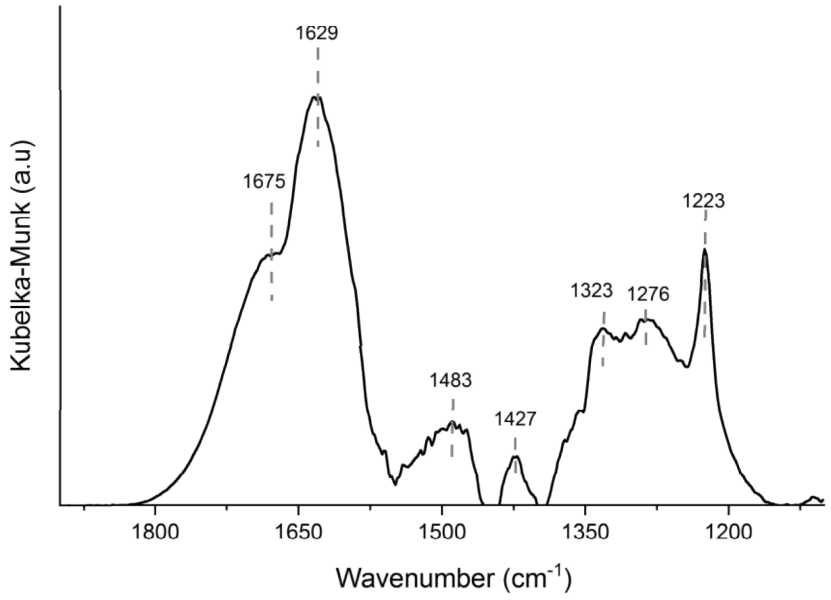


**Figure 33. 2000-1100 $cm^{-1}$ region DRIFTS subtraction spectrum of $ZrO_2$ NRs (**spectrum of the calcined sample subtracted from the $CO_2$ adsorption spectrum).

**Table 8. Surface species identified on observed wave numbers on $ZrO_2$ NRs**.

| Wavenumber (cm-1) | Species | References |
|---|---|---|
| 1629,1427,1223, 1276 | Bicarbonates | [9],[10] |
| 1483, 1323 | Mono and bidentate carbonates | [9] |

The subtraction spectrum was also obtained for the com $ZrO_2$ support, presented in Figure 34, to compare the difference in surface species formed after $CO_2$ adsorption on both the supports with the names of identified species and their IR wave-numbers in Table 9.

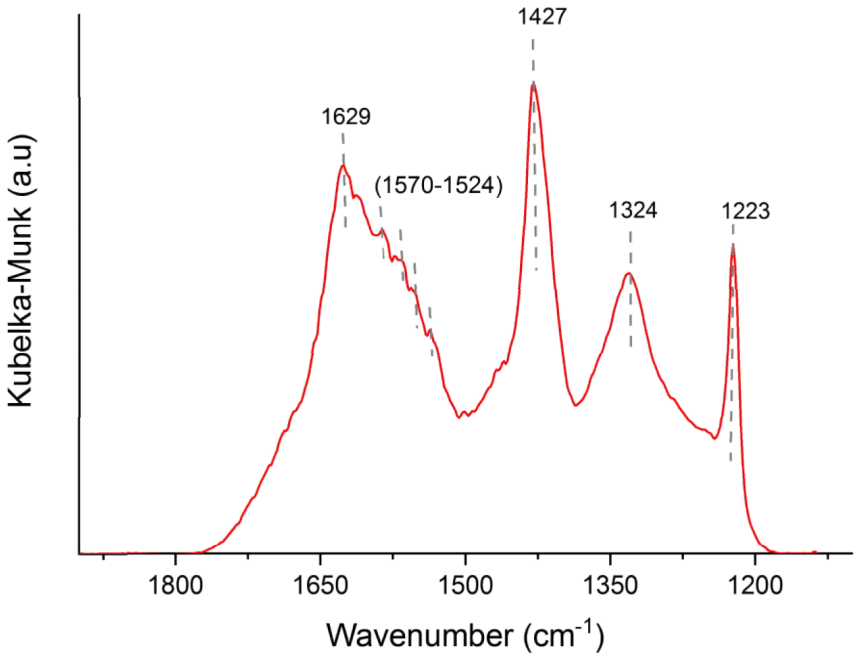


**Figure 34. 2000-1100 $cm^{-1}$ region DRIFTS subtraction spectrum of com $ZrO_2$** (spectrum of the calcined sample subtracted from the $CO_2$ adsorption spectrum).

**Table 9. Surface species identified on observed wave numbers on com $ZrO_2$.**

| Wavenumber ($cm^{-1}$) | Species | References |
|---|---|---|
| 1629,1427,1223 | Bicarbonates | [9],[10] |
| 1570-1524, 1323 | Mono and bidentate carbonates | [9] |

Combining the DRIFTS subtraction spectrum of both the supports with the identified carbon species and their wavenumbers is presented in Figure 35. From the figure, it confirmed the adsorbed $CO_2$ on both the support surface creates bicarbonates and mono-and bidentate carbonates. Such carbon species are formed differently and with different intensities on both the supports, relatively higher on com $ZrO_2$ support. Yet, some unidentified species in the bands between 1550-1300 $cm^{-1}$ in $ZrO_2$ NRs could be formates as many references reports [9].

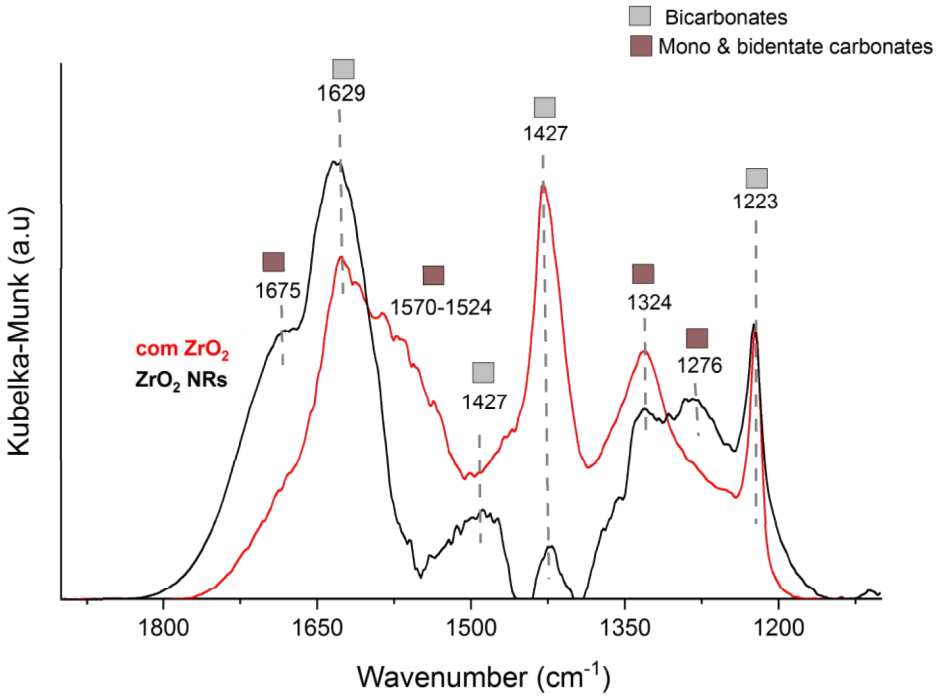


**Figure 35. DRIFTS subtraction spectrum of $ZrO_2$ NRs and com $ZrO_2$ and surface species comparison.**

***X-ray diffraction***

Repeating, the X-ray source during the XRD measurements was *Cobalt* and the XRD patterns are collected using Co Kα-1 radiation (1.789Å). Most of the references report the XRD patterns collected from Copper source using Cu Kα-1 radiation (1.541Å). To insure the XRD pattern measured using Co Kα-1 radiation matches the reference values, the diffraction angle (2θ) was re-calculated using equation 1 as described in Section 3.3.

To be noted, the lattice spacing (d) given in the equation 1 remains constant for the same sample even the X-ray source is changed. The High score plus software was used to obtain the lattice spacing (d) value measured with Co Kα-1 radiation and the diffraction angle (2θ) for Cu Kα-1 radiation was calculated using it. The measured and re-calculated diffraction angles are presented in Table 10 and the XRD patterns obtained in Figure 36.

Comparing the re-calculated diffraction angle (2θ) with Cu Kα-1 radiation with the references [1,62,27], assures the synthesized $ZrO_2$ NRs diffracted at the same value of diffraction angle (2θ) and were monoclinic in phase.

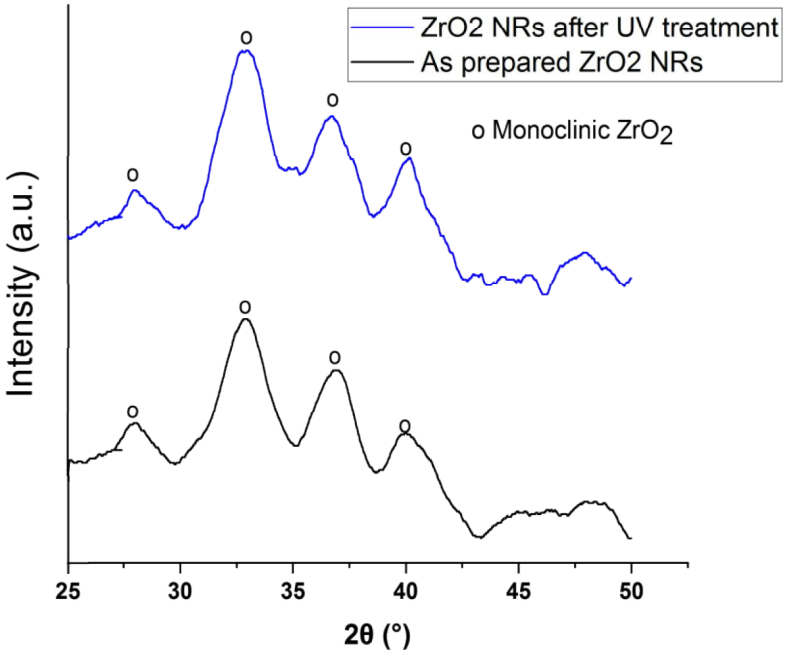


**Figure 36. XRD pattern obtained for $ZrO_2$ NRs using Co Kα-1.**

**Table 10. 2θ values with different X-ray sources.**

| | | | | |
|---|---|---|---|---|
| Measured 2θ using Co Kα-1 (°) | 27.9 | 32.7 | 35.9 | 40.2 |
| Re-calculated 2θ using Cu Kα-1 (°) | 25 | 28.1 | 31.2 | 34.3 |

***Nitrogen physisorption***

Table 11 lists the surface area, pore size, total and BJH pore volume of both the supports obtained from $N_2$ physisorption. From the result, the surface area of prepared $ZrO_2$ NRs and the BJH pore volume (mesopores) is comparatively higher than com $ZrO_2$ support indicating a good support for the catalyst. However, the pore diameter of both the support are significantly different in dimensions and for $ZrO_2$ NRs with the pore diameter of 2 nm around, it shows the pores in the support are in microspore size. Similarly, the total pore volume (micro+meso+macro pores) for $ZrO_2$ NRs is smaller than that in com $ZrO_2$. Concluding from the Table 9, with high surface area of $ZrO_2$ NRs, the pore sizes are very small in comparison to com $ZrO_2$ support.

**Table 11. Textural properties of zirconia supports, calcined at 350 °C.**

| Supports | Surface area ($m^2/g$) | Pore diameter (nm) | Total pore volume, $p/p^0$ =0.99 ($cm^3/g$) | BJH pore volume ($cm^3/g$) |
|---|---|---|---|---|
| $ZrO_2$ NRs | **193.25** | **2.06** | 0.21 | 0.45 |
| com $ZrO_2$ | **91.8** | **8.9** | 0.28 | 0.32 |

### 4.2.2 Rhodium loading and particle size

***$H_2$ chemisorption and X-ray fluorescence***

Results obtained from the $H_2$ chemisorption and XRF measurements are presented in Table 12. From the results, the Rh loadings (0.5 and 2 wt%) is higher in $ZrO_2$ NRs support than com $ZrO_2$ support. The dispersion of Rh in com $ZrO_2$ does not vary so much and neither the particle size with both the Rh loadings. Rh the particle size and the dispersion are significantly different in both the supports.

XRF measurements showed Rh loadings on 0.5Rh/$ZrO_2$ NRs catalyst is higher than 0.5Rh/com $ZrO_2$ catalyst as a result, the particle size should have increased in 0.5Rh/$ZrO_2$ NRs catalyst. With obtained results, even with higher loadings in 0.5Rh/$ZrO_2$ NRs catalyst the particle size is smaller in comparison to 0.5Rh/com $ZrO_2$ catalyst.

Noticeable from the table, 0.5Rh/$ZrO_2$ NRs resulted 105.5 % dispersion. Observing $H_2$ chemisorption isotherms in Appendix 1, the measurements data are reliable for this catalyst. Therefore, it was difficult to conclude the dispersion value exceeding 100 % but there can be single Rh atoms on the support accessible for $H_2$ chemisorption resulting higher dispersion. In this case, the stoichiometric factor could have been less than 2.

Catalyst characterization with TEM could be a better option for obtaining the reliable particle size and dispersion value. Adsorption isotherms obtained for all the catalysts is presented in Appendices 1 and 2.

**Table 12. Rhodium loading, dispersion and particle size in the catalysts.**

| Catalysts | Rh (wt %) | Rh dispersion (%) | Mean particle size (nm) |
|---|---|---|---|
| 0.5Rh/$ZrO_2$ NRs | 0.4 | 105.5 | **1.03** |
| 2Rh/$ZrO_2$ NRs | 1.4 | 29.2 | **3.7** |
| 0.5Rh/com $ZrO_2$ | 0.31 | 79.1 | **1.4** |
| 2Rh/com $ZrO_2$ | 1.0 | 67.6 | **1.6** |

### 4.2.3 Precursor decomposition

It was indeed an important analysis to determine the calcination temperature for the complete decomposition of precursor during the catalyst preparation procedure. From the TGA analysis results, in Figure 37, the degradation of precursor was observed most at 350 °C. It was confirmed that the temperature of 350 °C was enough for the catalyst calcination after loading the metal.

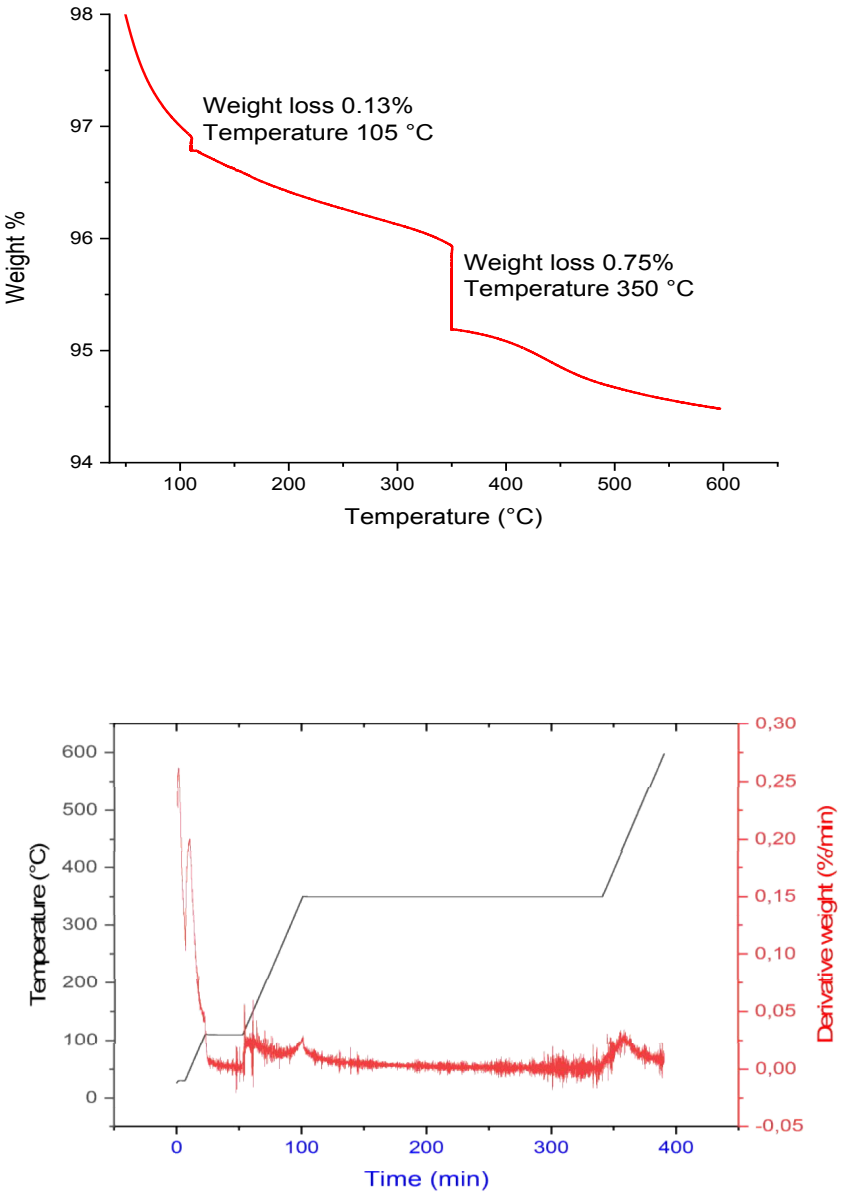


**Figure 37. TGA profiles of non-calcined 0.5Rh/com $ZrO_2$.**

## 4.3 Catalysts Activity

### 4.3.1 Conversions

The activity tests was carried out in $CO_2$ hydrogenation using two different Rh loaded catalysts prepared with com $ZrO_2$ and ZrO2 NRs supports. Figure 38 presents the activity and selectivity of the catalysts and numerical values with the standard deviations given in Table 13. Carbon monoxide (CO), methane ($CH_4$) along with the little amount of higher alkanes, ethane ($C_2H_6$) and propane ($C_3H_8$) were the main products detected by GC.

According to the figure, 0.5 Rh/com $ZrO_2$ catalyst showed the highest conversion. Catalysts prepared with $ZrO_2$ NRs support resulted lower conversion than with the com $ZrO_2$ support for both Rh loadings. With the higher loadings of Rh in both the catalysts, the conversions decreased slightly. In addition, Rh/com $ZrO_2$ is more selective towards $CH_4$ whereas, Rh/$ZrO_2$ NRs towards CO.

Interestingly, the selectivity towards higher alkanes, ethane and propane increased with higher metal loadings in Rh/$ZrO_2$ NRs than Rh/com $ZrO_2$. To be noted from XRF measurements, the particle size increased in 2Rh/$ZrO_2$ NRs and same catalyst resulted higher selectivity towards higher alkanes as well. It proves the $CO_2$ hydrogenation on this catalyst could have been due to dissociation of $CO_2$ into CO and O on the metal surface and further hydrogenated to longer chains of hydrocarbons. Lower loadings of Rh in $ZrO_2$ NRs is more selective towards $CH_4$, it can therefore be concluded that $ZrO_2$ NRs support favours lower loadings of Rh metal for better $CH_4$ yield.

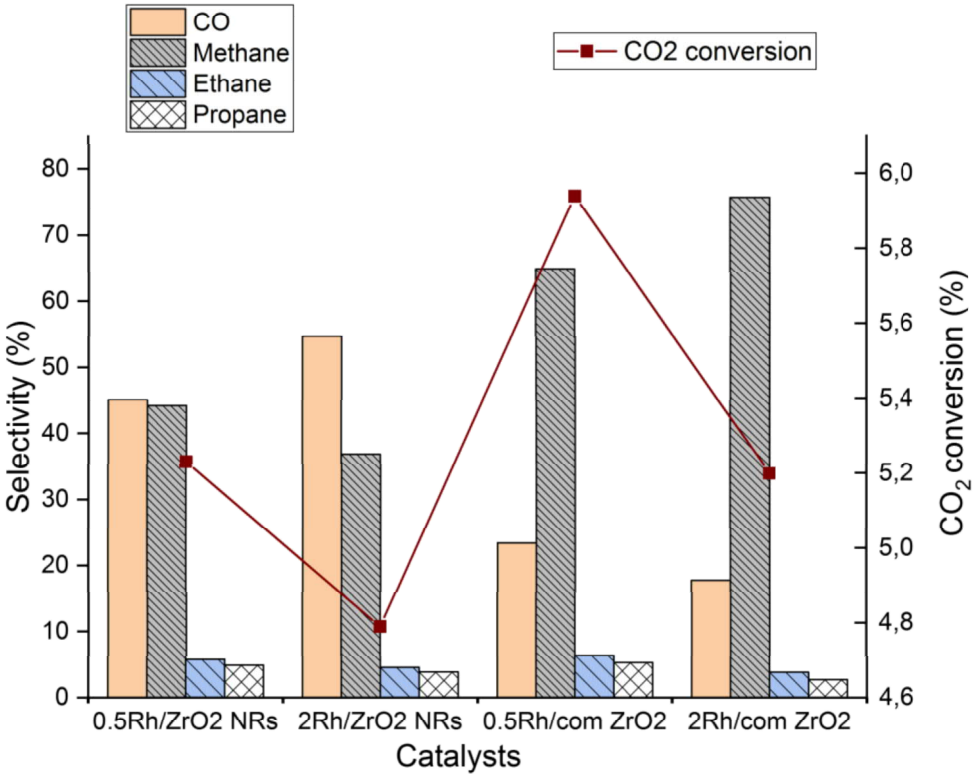


**Figure 38. Conversions and product selectivity by the catalysts in $CO_2$ hydrogenation; T= 200 °C, ambient pressure and $CO_2$:$H_2$ = 2:2.**

**Table 13. Conversions of catalysts in $CO_2$ hydrogenation.**

| Catalysts | Conversions (%) | Selectivity (%) | | | |
|---|---|---|---|---|---|
| | | Methane | CO | Ethane | Propane |
| 0.5 $Rh/ZrO_2$ NRs | 5.23 ± 0.1 | **44.2** | 45.1 | 5.8 | 4.9 |
| 2 $Rh/ZrO_2$ NRs | 4.79 ± 0.2 | **36.9** | 54.7 | 4.7 | 3.7 |
| 0.5 Rh/com $ZrO_2$ | 5.94 ± 0.1 | **64.9** | 23.4 | 6.4 | 5.3 |
| 2 Rh/com $ZrO_2$ | 5.20 ± 0.1 | **75.7** | 17.8 | 3.8 | 2.7 |

### 4.3.2 Products yields

$CH_4$ and CO yields by the catalysts in $CO_2$ hydrogenation is presented in Figure 39 and the numerical values in Table 14.

From the figure, $CH_4$ yield increased with the higher loadings of Rh in Rh/com $ZrO_2$ whereas, reverse in Rh/$ZrO_2$ NRs. The catalysts prepared with different supports resulted unsimilarity towards $CH_4$ yields.

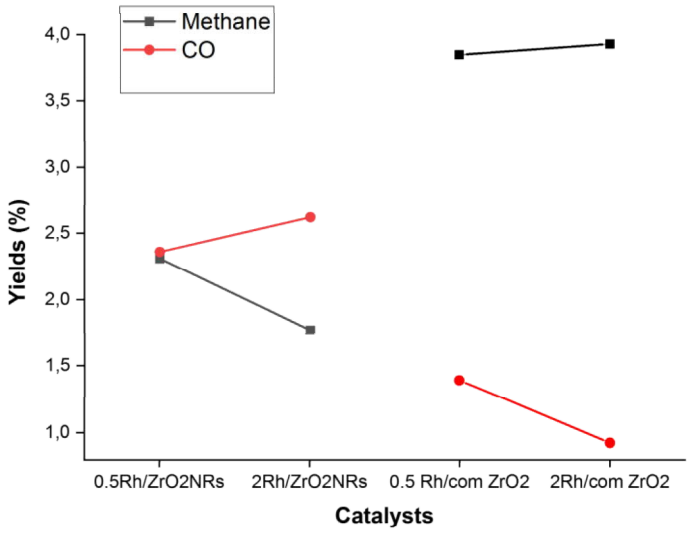


**Figure 39. Yields from the catalysts in $CO_2$ hydrogenation.**

**Table 14. Yields from the catalysts in $CO_2$ hydrogenation.**

| Products | Yields (%) | | | |
|---|---|---|---|---|
| | 0.5Rh/$ZrO_2$ NRs | 2Rh/$ZrO_2$ NRs | 0.5 Rh/com $ZrO_2$ | 2Rh/com $ZrO_2$ |
| Methane | **2.3** | **1.8** | **3.8** | **3.9** |
| CO | 2.4 | 2.6 | 1.4 | 0.9 |

### 4.3.3 Effect of WHSV

The effect of WHSV on the conversions of $CO_2$ was studied in the U-tube reactor, using 0.5Rh/com $ZrO_2$ with the feed compositions (2 vol% $CO_2$ and 2 vol% $H_2$), changing the total flow rates (40 ml/min and 25 ml/min) and the amount of catalysts (0.05 g, 0.2 g and 0.5g). Figure 40 clearly shows as the space velocity increased, conversions decreased.

The flow rates and amount of catalysts were changed to observe and overcome the internal mass transfer limitations in the U-tube reactor. Similarly, the conversions during the activity tests were intended to keep as low as possible. From the figure, the conversions were in between 5–6 % with different feeds and the same amount of catalysts. The products formed in every experiments analysed by GC were $CH_4$, CO, $C_2H_6$ and $C_3H_8$. It was clear that no mass transfer limitations existed in the U-tube reactor during the activity tests, therefore 0.2 g of catalysts with the WHSV between 1500 $h^{-1}$ and 6000 $h^{-1}$ was used during the activity tests of $Rh/ZrO_2$ NRs and Rh/com $ZrO_2$.

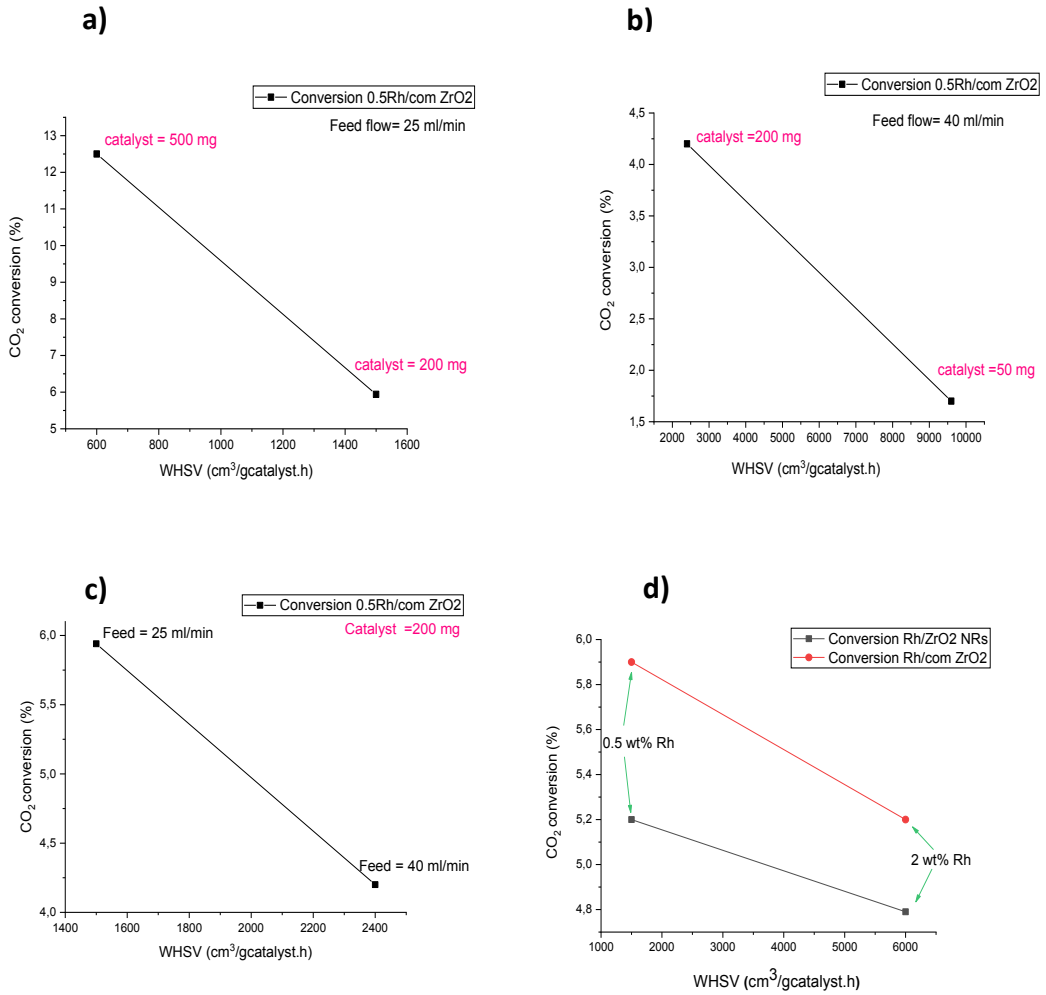


**Figure 40. Effect of WHSV on conversions** a) 0.5Rh/com $ZrO_2$ conversions; feed 25ml/min b) 0.5Rh/com $ZrO_2$ conversions; feed 40ml/min c) 0.5Rh/com $ZrO_2$ conversions; feeds 40 ml/min and 25 ml/min and 200 mg catalysts d) Rh/$ZrO_2$ NRs and Rh/com $ZrO_2$ conversions and WHSV in $CO_2$ hydrogenation.

*[During all reaction conditions and catalysts used, the final products detected were same: CO, methane, ethane and propane.]*

From Figure 41, the selectivity of the catalyst $Rh/ZrO_2$ NRs towards methane decreased with increasing WHSV and the catalyst Rh/com $ZrO_2$ resulted more selective towards methane.

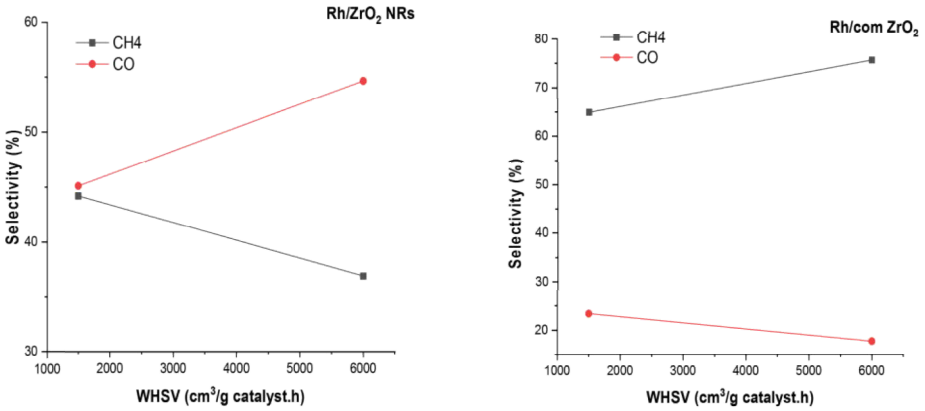


**Figure 41. The influence of WHSV on selectivity of the catalysts.**

### 4.3.4 Turn over frequency (TOF)

In Figure 42, TOF of Rh/ com $ZrO_2$ catalyst is comparatively higher than $Rh/ZrO_2$ NRs catalyst. TOF of $CO_2$ into $CH_4$ decreased with increase in particle size for the catalysts prepared with zirconia nanorods support. The particle size in com $ZrO_2$ only increased slightly, in turn the TOF is almost similar for both the loadings. The results could not answer clearly about less TOF of $Rh/ZrO_2$ NRs catalyst than Rh/com $ZrO_2$ catalyst, but some possible reasons of it and increase in particle size in $Rh/ZrO_2$ NRs will be discussed in Section 5.

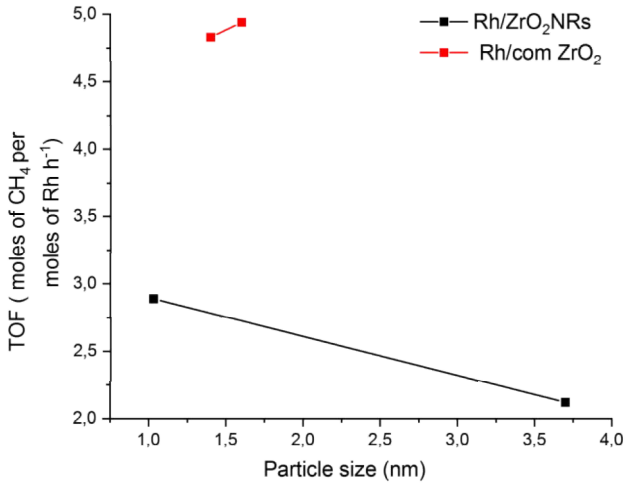


**Figure 42. The influence of Rh particle size on TOF.**

## 4.4 Estimation of the error

During this thesis work, the catalysts were characterised with different techniques and calculations were done from the results. The conversions and selectivity were calculated based on the results obtained from GC. The possible errors could have arise from the instrument or during the calculation.

To overcome the instrumental error, the measurements were carried out with the calibration of the equipment or handled by the responsible expert personnel during all experiments. During the reactions in AMI-200R, the flow of the gases could vary as a source error but it was checked with gas flow meter and made sure the flow was same during all the reactions. Another possibility could be due to the limitations in the instrument, poor working of the valves or the leakages. The valve connections in the instrument were checked by the responsible personnel to make sure no leakages occur and every valve were working properly. Repeatable experiments were carried out to obtain multiple data and results were based on the averages.

To overcome the calculation error, the characterization results were compared with the references and consulted to the experts in Aalto University. The conversion and selectivity were calculated based on the results obtained from the GC. Conversions and yield plots were made for every test using the data obtained from the GC. Unsimilar trend observed in the plots were neglected and averages were made out of the best one. One example presenting the excel sheet calculation is presented in Appendix 3.

# 5 DISCUSSIONS

## 5.1 Product formation and yields

$Rh/ZrO_2$, $metal/ZrO_2$ and Rh/metal oxides result in the formation of methane, higher alkanes, alcohols and aldehydes [11,23,30,37,41,79,81]. The prepared catalysts during this work resulted the formation of methane, CO and higher alkanes, in Figure 38 and Table 13.

DRIFTS results showed the surface hydroxyl groups were the main active sites for the reaction. The formation of higher alkanes could have involved the reaction scheme with CO formation mentioned in Section 2.2, which takes place with the dissociation of $CO_2$ into CO and O on the metal surface. Methane formation could have followed the routes involving the formation of carbonates, which was proven from the DRIFTS characterization where carbonate species were observed on zirconia support. Based on the formation of intermediate species and the products, the reaction scheme could be proposed for the $ZrO_2$ NRs in Figure 43 involving CO as intermediate forming longer carbon chains and in Figure 44 involving the carbonates as intermediate species following the methanation on the support surface.

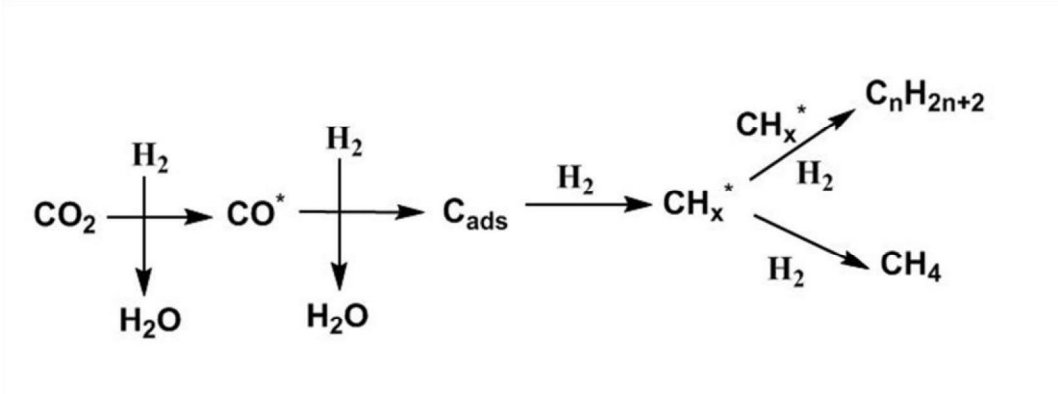


**Figure 43. Proposed reaction scheme involving CO as intermediate on $Rh/ZrO_2$,** adapted from references [26 & 44]**.**

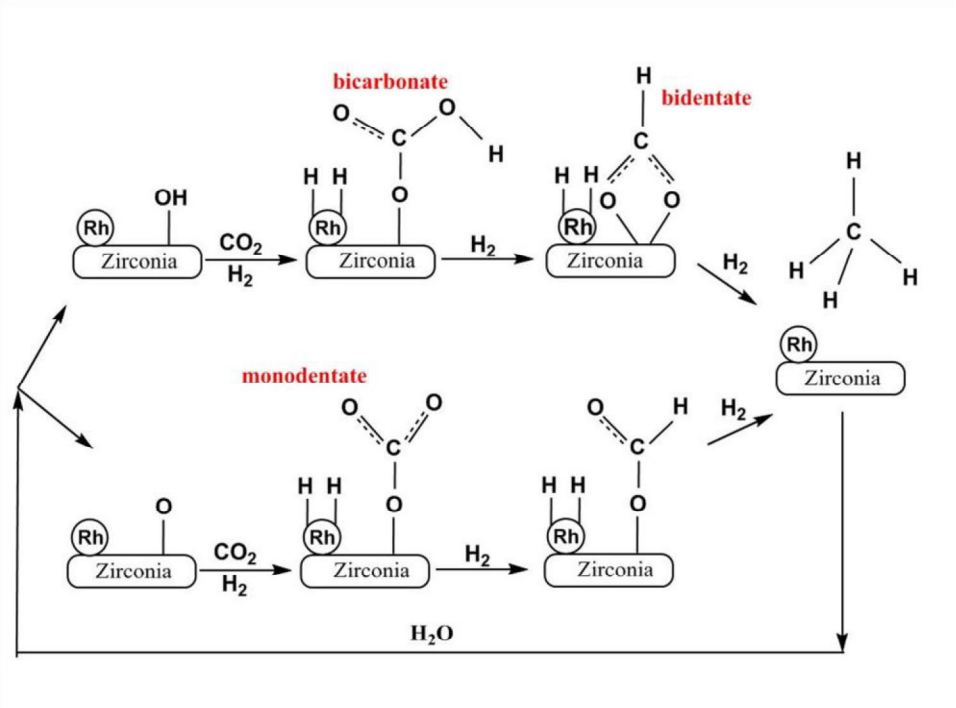


**Figure 44. Proposed reaction scheme involving carbonates as intermediate on $Rh/ZrO_2$ for methanation, adapted from** [82].

During $CO_2$ hydrogenation, WHSV and the metal loadings on the catalysts were two variables employed. The catalyst with $ZrO_2$ NRs support resulted lower methane yields in both the conditions. Section 5.2 describes more about the support surfaces and possible reasons for less methane yields.

## 5.2 Effect of the support

DRIFTS characterization in Section 4.2, resulted the difference in the $CO_2$ adsorption and formation of the intermediate species on $ZrO_2$ NRs and com $ZrO_2$ surfaces. Higher $CO_2$ adsorption on com $ZrO_2$ resulted better $CO_2$ conversion in hydrogenation reaction, as expected.

Although UV treatment ensured the oleate removal from the $ZrO_2$ NRs surface, the XPS results cannot be ignored which showed Na and C on the support surface,

which could be remains of oleate traces. Similarly, in Figure 45 the appearance of C-H stretch in DRIFTS spectra after calcination at 350 °C proves the oleate (carbon) remains on the support surface. Extra DRIFTS experiment was carried out during this work where $ZrO_2$ NRs support was calcined at 450 °C. After calcination at 450 °C the C–H region disappeared in the spectrum indicating the surface oleate was removed completely.

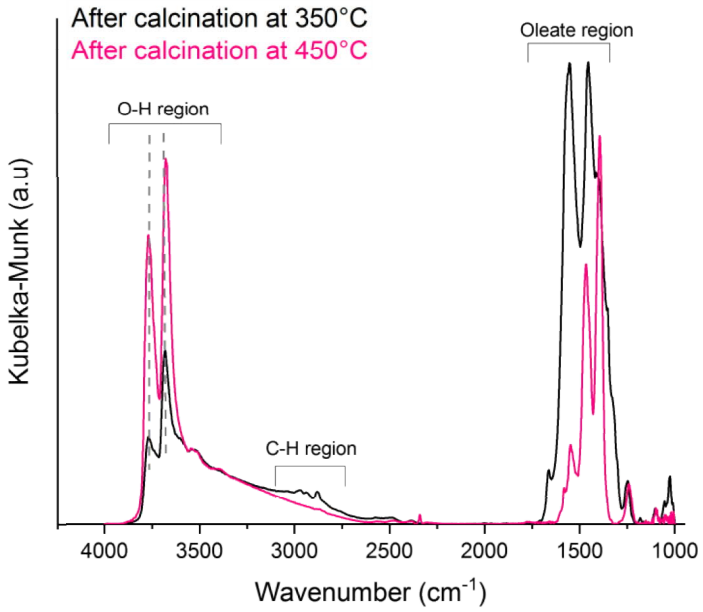


**Figure 45. The influence of calcination temperature on $ZrO_2$ NRs surface.**

Figure 45 provides another essential information that the intensity of OH groups increased with the disappearance of the C–H region and the bands of the oleate changed with the calcination temperature to 450 °C. This result proves that the carbon deposits on $ZrO_2$ NRs surface could have occupied the surface hydroxyl groups. Occupied surface hydroxyl groups by carbon could be the reason for less $CO_2$ adsorption on $ZrO_2$ NRs less than on com $ZrO_2$ support that resulted less methane yield in $CO_2$ hydrogenation.

During the DRIFTS experiment, $ZrO_2$ NRs and com $ZrO_2$ supports were characterized at 450 °C calcination temperature and DRIFTS subtraction spectra (the spectrum after calcination subtracted from the $CO_2$ adsorption spectrum) for both the support was obtained, in Figure 46.

From the figure, the $CO_2$ adsorbed on $ZrO_2$ NRs is higher in intensity than on com $ZrO_2$. The desorption of $CO_2$ from the support should be checked with increasing temperature to proceed with this work. These results look promising for better $CO_2$ conversion for zirconia nanorods supported catalyst.

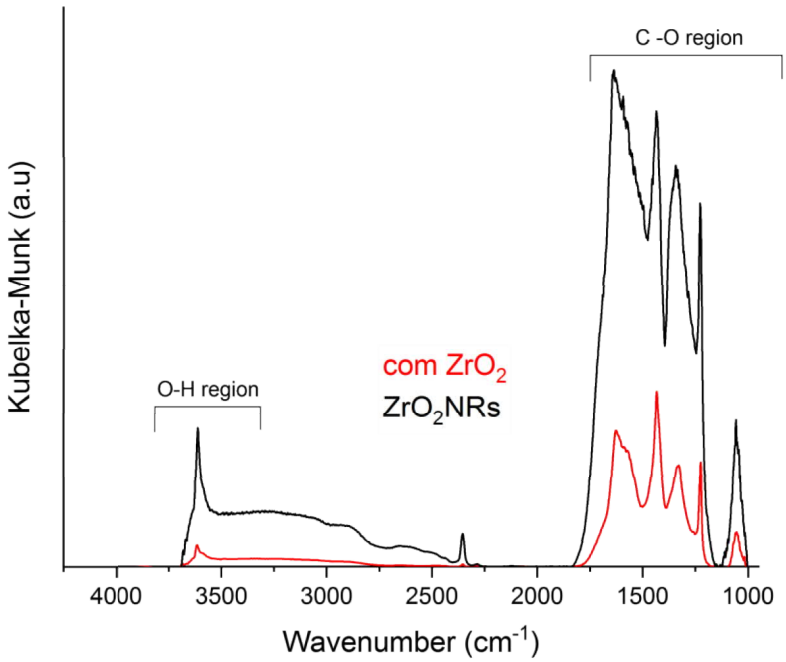


**Figure 46. DRIFTS subtraction spectra of the both supports calcined at 450 °C.**

Sorption experiments showed difference in the surface area of both the supports, where the surface area of $ZrO_2$ NRs was almost twice than the com $ZrO_2$ support in Section 4.2.2 (Table 11). Very small pore sizes and volume in $ZrO_2$ NRs was another

thing to be taken in account. The change in the surface area after loading the metal would have been a wise option to check if these pores were blocked by the metal particles.

## 5.3 Effect of the Rh particle size

The Rh particle size and loadings on both the supports, Section 4.2, was unsimilar thus resulting $CO_2$ conversions and selectivity were unalike. In com $ZrO_2$ support, the Rh particle sizes are almost same even with higher metal loadings and smaller as well compared to $ZrO_2$ NRs support. As a result, Rh/com $ZrO_2$ catalyst showed higher conversion and methane selectivity.

Interestingly, XRD results showed higher metal loading on $ZrO_2$ NRs than on com $ZrO_2$ support with 0.5 wt% loading of Rh. Single atoms as well as the particle Rh on $ZrO_2$ NRs could be a possible reason for higher loading. With increasing loadings to 2 wt%, the dispersion decreased with increasing Rh particle size on Rh/$ZrO_2$ NRs. Less available surface sites on $ZrO_2$ NRs surface could have resulted in less dispersion and increase in particle size. As described in Section 5.2, the surface sites (surface hydroxyl groups) seems to be occupied by carbon deposits and in result with the higher loadings of Rh on $ZrO_2$ NRs; Rh particle could have agglomerated forming the bigger particle sizes. With the bulk structure, it could be possible not all Rh atoms being accessible to the reactants and products formation, the conversion and methane selectivity of Rh/$ZrO_2$ NRs decreased as mentioned in Section 4.3.1 (Figure 38).

# 6 CONCLUSIONS AND PERSPECTIVES

The scope of this present work was to study the activity of two different structured Rh/zirconia catalysts in $CO_2$ hydrogenation. The activity of the catalyst Rh/$ZrO_2$ NRs was tested and compared with Rh/com $ZrO_2$ catalyst in $CO_2$ hydrogenation. As a result of this work, it can be stated the structure of the support played an important role in the catalyst activity.

Monoclinic zirconia nanorods, calcined at 350 °C showed very interesting features with the high surface area, pore sizes and the actives sites (surface hydroxyl groups). It can be accepted that the surface hydroxyl groups on monoclinic zirconia support was the main active site for the reaction based on DRIFTS characterization experiments. It also provided qualitative and quantitative information on the adsorption of $CO_2$ on both the supports, comparatively less on $ZrO_2$ NRs support. The possible reason could be the remains of oleate on $ZrO_2$ NRs support observed from DRIFTS spectra. These oleate could have occupied the surface sites on the support resulting less adsorption of $CO_2$.

0.5 and 2 wt% Rh was loaded on the supports by wet impregnation. Interestingly, the characterization results from XRF and $H_2$ chemisorption showed higher Rh loadings and the particle size on Rh/$ZrO_2$ NRs catalyst than Rh/com $ZrO_2$ catalyst. Increasing Rh loading on both the supports, $ZrO_2$ NRs support bigger particle size was observed on $ZrO_2$ NRs support whereas, on com $ZrO_2$ support the particle size merely differed.

As a result, in $CO_2$ hydrogenation methane was the main product along with small amount of higher alkanes and CO. The activity of Rh/$ZrO_2$ NRs for methane formation was lower than Rh/com $ZrO_2$. The methane yield decreased further with the higher loadings of Rh on Rh/$ZrO_2$ NRs but increased on Rh/com $ZrO_2$.

Concluding the work, the structure of the catalyst is likely to influence the activity and selectivity in $CO_2$ hydrogenation. The presented results are useful for the future work, but further catalyst characterization is necessary. Oleate removal from the $ZrO_2$ NRs support could be the prior step to continue and catalysts preparation with other loadings (preferably less Rh loadings) on the support could be a wise option to get comparable results. The increase in catalyst calcination temperature and reaction temperature could be other options as well.

As future perspective, grinding nanorods into very fine powder during the exposure to UV-ozone treatment and TGA characterization are the aspects for the oleate removal and to obtain clean support sample.

Nevertheless, the activity tests of the catalyst was intended to perform with the catalyst calcination at 350 °C. In future, the catalyst could be calcined at 450 °C as mentioned in sub-section 5.2. Increasing temperature could result in the phase of the support, from monoclinic to tetragonal, where XRD characterization could be an option to quantify the monoclinic and tetragonal phases.

Dispersion of the metal and the metal particle size needs further characterization to obtain more accurate results. TEM technique could be performed to obtain the particle size distribution histogram as well as visualizing the position of the metal on the catalyst surface.

In addition, the reaction mechanism of Rh/zirconia catalyst in $CO_2$ hydrogenation can be investigated via DRIFTS with MS characterization.

# REFERENCES


1 Wang, W. & Gong, J. *Front. Chem. Sci. Eng*, **2011**, 5(1), 2–10.

2 Sakakura, T. & Kohno, K. Chem. Commun., **2009**, 1312–1330.

3 Sahebdelfar, S. & Ravanchi, M.T. *Journal of Petroleum and Science and Engineering* 134, **2015**, 14–22.

4 Jalama,K. *CATALYSIS REVIEWS*, **2017**, 59, NO.2,95–164.

5 Omae, I. *Catalysis Today*, **2006**, 115, 33–52.

6 Aziz,M.A.A., Jalil, A.A., Triwahyono, A., & Ahmad, A. *Green Chem*. **2015**, *17*, 2647–2663.

7 Abe, T., Tanizawa, M., Watanabe, K. & Taguchi, A. *The Royal Society of Chemistry*, **2009**, 315–321.

8 Gutiérrez, A. Aalto University Doctoral Dissertations 140, **2013**.

9 Kouva, S., Andersin, J., Honkala, K., Lehtonen, J., Lefferts, L., & Kanervo, J. *Phys. Chem. Chem. Phys.*, **2014**, 16, 20650-20664.

10 Kouva, S., Honkala, K., Lefferts, L., & Kanervo, J. *Catal. Sci. Technol.*, **2015**, 5, 3473-3490.

11 Wambach, J., Baiker, A. & Wokaun, A. *Phys. Chem.*, **1999**, 1, p. 5071-5080.

12 Goharshadi, E.K. & Hadadian, M. *Ceramics International* 38, **2012**, 1771–1777.

13 González, R.A., Diaz-Droguett, D.E., Avila, J.I., González, C.A. & Fuenzalida, V.M. *Materials Letters* 65, **2012**, 2121–2123.

14 Fechete, I. & Vedrine, C.J. *Molecules*, **2015**, 20(4), 5638–5666.

15 Chen, A., Zhou, Y., Miao, S., Li, Y. & Shen, W. *CrystEngComm*, **2016**, 18, 580-587.

16 Bruno, T., Beretta, A. & Groppi, G. *Catalysis Today*, **2005**, 89.

17 Rönsch, S., Schneider, J., Matthischke, S., Schluter, M., Gotz, M.,Lefebre, J., Prabhakaran, P. & Bajohr, S. Review on methanation—From fundamentals to current projects. *Fuel* **2016**, *166*, 276–296.

18 Vlasenko, V.M., Yuzefovich, G.E. *Russ. Chem. Rev.* **1969**, 38(9), 728–739.

19 Wang, W., Wang, S., Ma, X. & Gong, J. *Chem. Soc. Rev*, **2011**, 40(7), 3369–4260.

20 Marwood, M., Doepper, R. & Renken, A. *Applied Catalysis A: General*, 151, **1997**, 223–246.

21 Centi, G. & Perathoner, S. *Catalysis Today*, 148, **2009**, 191–205.

22 Stangeland, K., Kalai, D., Li, H. & Yu, Z. *Energy Procedia*, 105, **2017**, 2022–2027.

23 Jacquemin, M., Beuls, A. & Ruiz, P. *Catalysis Today*, 157, **2010**, 462–466.

24 Langmuir, I. *J.Am. Chem. Soc.,* 37, **1915**, 1139.

25 Langmuir, I. *Trans. Faraday. Soc.,* 17, **1922**, 607.

26 Kusama, H., Okabe, K., Sayama, K. & Arakawa, H. *Energy*, 22, **1997**, 343–348.

27 Bachiller-Baeza, B., Rodriguez-Ramos, I. & Guerrero-Ruizs, A. Langmuir, **1998**, 14, 3556–3564.

28 Guglielminotti, E. Langmuir, **1990**, 6, 1455–1460.

29 Etrl, G., Knözinger, H., Schüth, J. & Weitkamp, J. Handbook of Heterogeneous Catalysis, Volume 1.

30 Gogate, M.K. & Davis, R.J. *Catalysis Communications*, 11, **2010**, 901–906.

31 Vogt, C., Groeneveld, E., Kamsma, G., Nachtegaal, M., Lu, L., Kiely, C.J., Berben, P.H., Meirer, F. & Weckhuysen, B.M. *Nature Catalysis*, 1, **2018**, 127–134.

32 Cai, M., Wen, J., Chu, W., Cheng, X. & Li, Z. *Journal of Natural Gas Chem.*, **2011**, 20, 318–324.

33 Yamasaki, M., Habazaki, H., Asami, K., Izumiya, K. & Hashimoto, K. *Catalysis Communications*, 7, **2006**, 24–28.

34 Ren, J., et al. *Fuel Cell Processing Technology*, **2015**, 137, 204–211.

35 Tada, S., et al, *International Journal of Hydrogen Energy*, **2014**, 39, 10090–10100.

36 Tada, S., et al, *International Journal of Hydrogen Energy*, **2012**, 37, 5527–5531.

37 Lange, F., Armbruster, U. & Martin, A. *Energy Technology*, **2015**, 3, 55–62.

38 Fujita, S.-i., Moribe, S., Kanamori, Y., Kakudate, M. & Takezawa, N. *Applied Catalysis*, A: General, **2001**, 207, 121–128.

39 Inoue, T. & Iizuka T. *J. Chem. Soc., Faraday Trans*. 1, **1986**, 82, 1681–1686.

40 Fujita, S., Usui, M., Hananda, H. & Takezawa, N. *React. Kinet. Catal. Lett*., **1995**, 56, 15–19.

41 Fisher, I.A. & Bell, A.T. *Journal of Catalysis*, **1996**, 162, 54–62.

42 Martin, D. & Duprez, D. Applied Catalysis A: General, **1995**, 131, 297–307.

43 Wang, J.A., López, L., Bokhimi, X. & Novaro, O. *Journal of Molecular Catalysis A: Chemical 239*, **2005**, 249–256.

44 Chen, W., Ding, Y., Song, X., Wang, T. & Luo, h. *Applied Catalysis A: General 407*, **2011**, 231–237.

45 Burch, R. & Loader, P.K. *Applied Catalysis A: General 143*, **1996**, 317–335.

46 Gandhi, H.S., Graham, G.W. & McCabe, R.W. *Journal of Catalysis*, 216, **2003**, 433–442.

47 Huo, Z., Chen, P., Fang, H., Zheng, X. & Yashima, T. *International Journal of Hydrogen Energy*, 31, **2006**, 555–561.

48 Wang, C., et al, *Applied Catalysis A General,* 544, **2017**, 30–39.

49 Deutschmann, O., Knözinger, K., Kochloefl, K. & Turek, T. Weinheim, Wiley-VCH Verlag GmbH & Co. KGaA, **2009**.

50 Lim, Y., McGregor, J., Sederman, A.J., et al. *Chemical Engineering Science*, 141, 28-45.

51 Thomas, J.M & Thomas, J.W. *Principles and Practice of Heterogeneous Catalysis*, **1996**.

52 Karelovic, A. & Ruiz, P. *Journal of Catalysis*, 301, **2013**, 141–153. (Rh/TiO2)

53 Panagiotopoulou, P. *Applied Catalysis* A, General 542, **2017**, 63–70. (Rh/TiO2).

54 Yamaguchi, T. *Catalysis Today*, 20, **1994**, 199–217.

55 Gosku, H., Sert, H., Kilbas, B. & Sen, F. *Current Organic Chemistry*, **2017**, 21, 9.

56 Richardson, J.T. Principles of Catalyst Development, Fundamental and Applied Catalysis, **1989**.

57 El-Ghany, O.S. & Sherief, A.H. *Future Dental Journal*, **2016**, 2, 55–64.

58 Piconi, C. & Maccauro, G. *Biomaterials*, **1999**, 20, 1–25.

59 Kelly, J.R. & Denry, I. *Dental Materials*, **2008**, 24, 289–298.

60 EPA Chemicals under the TSCA, **2018**. [Online]. Available: http://www.epa.gov/chemicals-under-tsca

61 USGS, Mineral Commodity Summaries, **2017**.

62 Viinikainen, T., Rönkkönen, H., Bradshaw, H., Stephenson, H., Airaksinen, S.,Reinikainen, H., Simell, P., & Krause, O. *Applied Catalysis A: General* 362, **2009**,169–177.

63 Materials Design, Temperature-Dependent Phase Transitions of $ZrO_2$, **2009**.

64 Jung, K.T., Shul, Y.G. & Bell, A.T. *Catal. Lett.,* **1997**, 44, 11–17.

65 Goharshadi, E.K. & Hadadian, M. *Ceramics International*, **2012**, 38, 1771–1777.

66 González, R.E., Mosquera, E., Mogila, I., Villarroel, R. & Fuenzalida, V.M. *Ceramics International,* **2014**, 40, 15577–15584.

67 Asemani, H.R., Sarabi, A.A., Mohammadloo, H.E. & Sarayloo, M. *J. Coat. Technol. Res.*, **2016**, 13, 883–894.

68 Eichler, J., Eisele, U. & Rödel, J. *J. Am. Ceram. Soc*., **2004**, 87, 1401–1403.

69 Khan, A.S., Fu, Z., Rehman, A.S., Asif, M., Wany, A. & Wang, H. *Powder Technology,* **2014**, 256, 71–74.

70 Liu, Y. et al, *J. Am. Ceram. Soc*., **2002**, 85, 3120–3122.

71 Hakeem, A.A., et al, *Journal of Catalysis*, **2014**, 313, 34–45.

72 Kockmann, A., Hesselbach, J., Zellmer, S., Kwade, A. & Garnweitner, G. RSC Adv., **2015**, 5, 60993.

73 Su, J., Li, Y., Yan, X. & Li, R. *Chemical Physics Letters*, **2016**, 650, 98–101.

74 Sliem, M.A., et al, *Chem Mater.,* **2012**, 24, 4274-4282.

75 Wan, C., Lu, Y., Sun, Q. & Li, J. Applied Surface Science, **2014**, 321, 38–42.

76 Dudnik, E.V. *Powder Metallurgy and Metal Ceramics*. **2009**, vol. 48.

77 Kwasny, J. & Balcerzak, W. *Technical Transitions 2*, Environmental Engineering, **2017**.

78 Marceau, E., Carrier, X. & Che, *M. Wiley-VCH Verlag GmbH & Co. KGaA*, **2009**, 59–82.

79 Qihai, L., Xinfa, D. & Zili, L. *Chinese Journal of Chemical Engineering*, **2014**, 22, 131–135.

80 Harju, H., Lehtonen, J. & Lefferts, L. *Applied Catalysis B: Environmental 182*, **2016**, 33–46.

81 Inoue, T., Iizuka, T. & Tanabe, K. *Applied Catalysis*, **1989**, vol. 46, 1–9.

82 Schild, C. & Wokaun A. *J. Phys. Chem*., **1991**, 95, 6341–6346.

83 Pan, Q., Peng, J., Sun, T., Wang, S. & Wang, S. Catalysis Communications, **2014**, 45, 74–78.

84 Niemantsverdriet, J.W. Spectroscopy in Catalysis, *Handbook 3rd edition*, **2007**.

85 Khokhlov, A.G., Valiullin, R.R., Stepovich, M.A. *Colloid Journal*, **2008**, vol. 70, 507-514.

86 Barrett, E.P, Joyner, L.G., & Halenda, P.P. *American Chemical Society*, **1951**, vol.61, p.373.

87 Boudart, M., & Djega-Mariadassou, G. *Kinetics of Heterogeneous Catalytic Reactions*, **1984**.

88 Roonasi, P., Yang, X., & Holmgren, A. *Journal of Colloid & Interface Science* 343, **2010**, p. 546-552.

# APPENDICES

APPENDIX 1. $H_2$ adsorption isotherms obtained for a) 0.5Rh/$ZrO_2$ NRs b) 2Rh/$ZrO_2$ NRs.

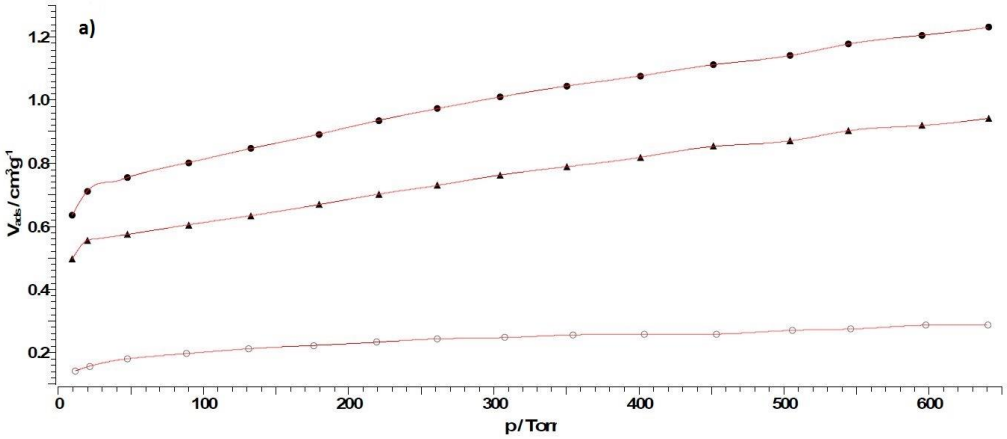


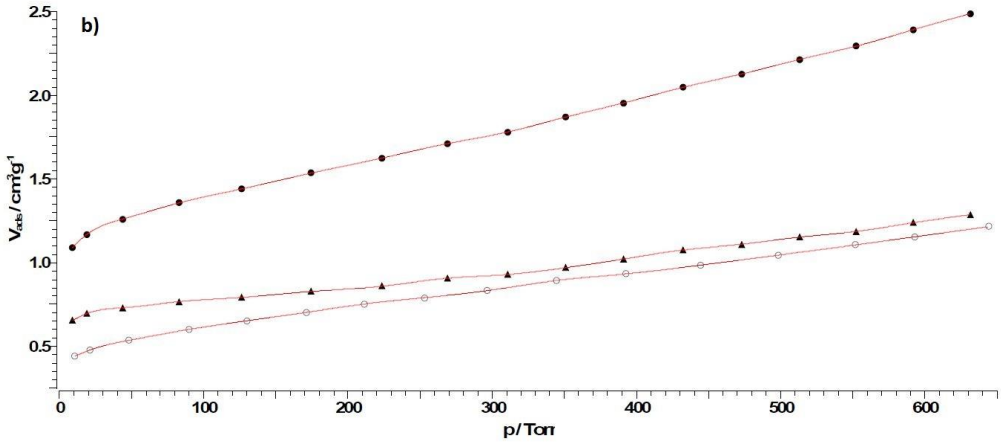

# APPENDICES

APPENDIX 2**.** $H_2$ adsorption isotherms obtained for a) 0.5Rh/com $ZrO_2$ b) 2Rh/com $ZrO_2$.

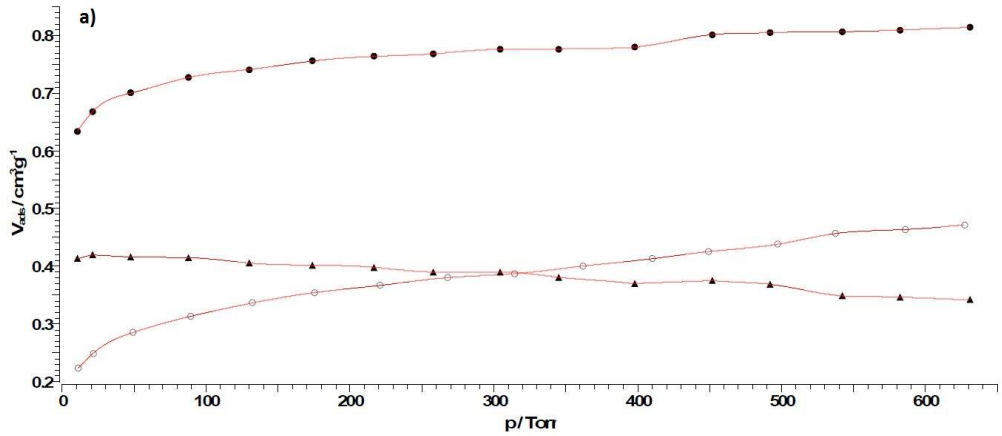


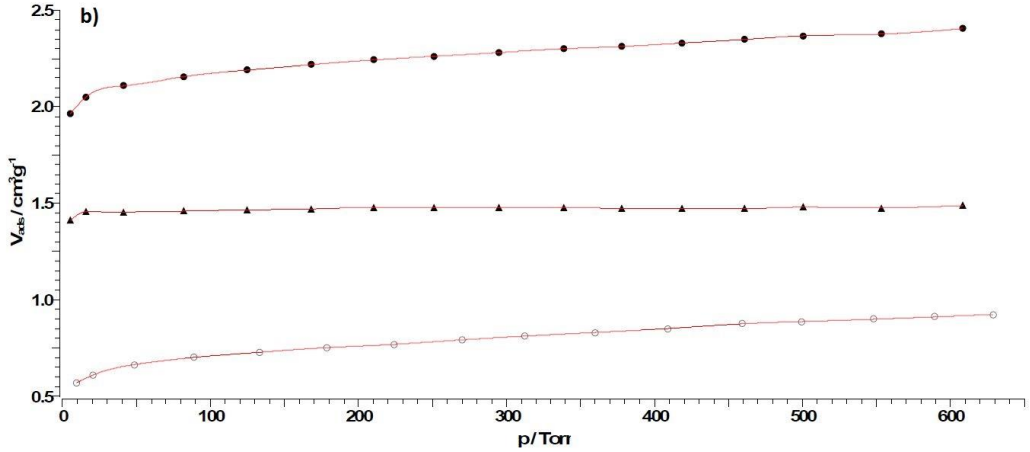

# APPENDICES

APPENDIX 3. An example of excel sheet showing the conversion calculations from the results obtained from GC.